JEM Journal of Experimental Medicine

ARTICLE

Nicotine promotes brain metastasis by polarizing microglia and suppressing innate immune function

Shih-Ying Wu[1], Fei Xing[1], Sambad Sharma[1], Kerui Wu[1], Abhishek Tyagi[1], Yin Liu[1], Dan Zhao[1], Ravindra Pramod Deshpande[1], Yusuke Shiozawa[1], Tamjeed Ahmed[2], Wei Zhang[1], Michael Chan[4], Jimmy Ruiz[2,3], Thomas W. Lycan[2], Andrew Dothard[2], and Kounosuke Watabe[1]

Up to 40% of lung cancer patients develop brain metastasis, and the median survival of these patients remains less than 6 months. Smoking is associated with lung cancer. However, how smoking impacts the development of brain metastasis remains elusive. We examined 281 lung cancer patients with distant metastasis and found that smokers exhibited a significantly high incidence of brain metastasis. We found that nicotine enhanced brain metastasis, while a depletion of microglia suppressed this effect in vivo. Nicotine skewed the polarity of microglia to the M2 phenotype, thereby increasing the secretion of IGF-1 and CCL20, which promoted tumor progression and stemness. Importantly, nicotine enhanced the expression of SIRPα in microglia and restricted their phagocytic ability. We also identified a compound, parthenolide, that suppressed brain metastasis by blocking M2 polarization. Our results indicate that nicotine promotes brain metastasis by skewing the polarity of M2 microglia, which enhances metastatic tumor growth. Our results also highlight a potential risk of using nicotine for tobacco cessation.

Introduction

Approximately 170,000 patients in the United States are diagnosed with brain metastasis every year (Ellis et al., 2012). Lung, breast, and skin cancers are the most common tumor types that metastasize to the brain (Bacha et al., 2018; Huang et al., 2018; Redmer, 2018; Xing et al., 2018). Patients with metastatic lung cancer have a very poor prognosis (Mujoomdar et al., 2007), and those with brain metastasis have a 1-yr survival rate of 4–20% (Gaspar et al., 1997; Sperduto et al., 2008; Verger et al., 2005). Despite significant improvements in the treatment of metastatic cancer, the therapeutic options for brain metastasis are still limited mainly due to inefficient drug delivery to brain as well as limited surgical approaches to multiple metastases. Radiation therapies, such as stereotactic radio surgery and fractionated whole brain radiation, are standard therapeutic techniques employed for brain metastasis; however, they provide only limited local tumor control and, more often than not, intracranial failure leading to neurological death. The development of lung cancer brain metastasis is a complex process, requiring the invasion of primary tumor cells into surrounding tissue and vessels, trafficking through the circulatory system, and colonizing into the brain parenchyma (Fidler, 2015). Therefore, understanding the underlying mechanisms that drive brain metastasis and developing more effective therapies are urgently needed.

Cigarette smoking is one of the major risk factors for lung cancer (Lee et al., 2012). Our previous study have shown that smoking is correlated to rapid progression of lung cancer brain metastasis (Shenker et al., 2017). Tobacco smoke contains a toxic mix of >7,000 chemicals. Among them, nicotine is a major cigarette component associated with human tobacco consumption and addiction (Braverman, 1999; Heishman, 1999). Nicotine is not a carcinogen; however, several studies have reported the tumor-promoting effects of nicotine via activation of nicotinic acetylcholine (nAch) receptor in the tumor cells. The nAch receptor is comprised of combination of multiple subunits, and they are expressed in a variety of brain cells including neuron, astrocytes, endothelial cells, and microglia (Mazzaferro et al., 2017). The α4β2 is the most abundant class of nAch receptor in the brain and is the principal mediator of nicotine dependence (Hawkins et al., 2004; Mazzaferro et al., 2017). This suggests that nicotine may be capable of reprogramming the brain tumor microenvironment (TME) via activation of its receptor to promote tumor progression.

Several studies have shown that the interaction of neoplastic cells with microglial cells, brain-residing macrophages, profoundly

[1]Department of Cancer Biology, Wake Forest Baptist Medical Center, Winston-Salem, NC; [2]Department of Medicine, Section of Oncology and Hematology, Wake Forest Baptist Medical Center, Winston-Salem, NC; [3]Section of Hematology and Oncology, W.G. (Bill) Hefner VA Medical Center, Salisbury, NC; [4]Department of Radiation Oncology, Wake Forest Baptist Medical Center, Winston-Salem, NC.

Correspondence to Kounosuke Watabe: kwatabe@wakehealth.edu.

affects tumor progression in glioblastoma (da Fonseca and Badie, 2013; Roesch et al., 2018; Wei et al., 2013). In brain metastatic lesions of lung cancer patients, abundant activated microglia were found to be infiltrated (He et al., 2006). Importantly, nAch receptor has been shown to be expressed on microglia (Morioka et al., 2015; Sadigh-Eteghad et al., 2016), raising the possibility that nicotine may stimulate microglia's immunomodulatory pathways, which affects their immune function. Microglia are known to polarize into classical (M1) or alternative (M2) phenotypes by various microenvironment stimuli (Wei et al., 2013; Wu and Watabe, 2017). M1 cells suppress tumors by releasing cytotoxic factors and also by phagocytosis. In contrast, M2 cells have a pro-tumor response by activating immunosuppressive factors. It is virtually unknown how metastatic cells escape immune attack of microglia and then colonize in the brain. In this study, we showed that nicotine promoted lung cancer brain metastasis by enhancing both tumor progression and stemness by skewing microglial polarization and inhibiting its anti-tumor phagocytic ability. We also found that a natural compound, parthenolide (PTL), effectively suppressed tumor progression and stemness by blocking nicotine-induced polarization of the microglia in the brain.

Results

Smoking increases brain metastasis of lung cancer

To examine the effect of tobacco smoking on brain metastasis, we analyzed the incidence and mortality rate of 281 patients with lung cancer brain metastasis (Fig. S1) with or without a history of smoking. All patients were diagnosed with stage IV disease. Among them, 79 patients were diagnosed with brain metastasis. 59 patients were current smokers at the time of diagnosis and treatment, while 222 of them had either a previous or no smoking history. We found that the incidence of brain metastasis was significantly higher in current smokers compared with the never or the former smokers group (Fig. 1 A). The results of Kaplan–Meier analyses indicate that the current smokers were associated with worse brain metastasis progression free (Fig. 1 B) and overall survival (Fig. 1 C) compared with those who were not currently smoking. Since activation of microglia was previously reported to be associated with brain tumor progression (da Fonseca and Badie, 2013; He et al., 2006; Roesch et al., 2018; Wei et al., 2013), we examined the status of microglia activation in brain metastatic lesions and found that current smokers exhibited a significantly increased number of Iba1$^+$ (pan-microglial marker) cells in the brain metastatic lesions (Fig. 1 D) compared with noncurrent smokers. Importantly, the majority of infiltrated microglia in current smokers was identified to be pro-tumor M2 microglia (CD206$^+$ cells; Fig. 1 D). These results suggest a role of smoking-mediated M2 microglial polarization in brain metastatic tumor growth.

Nicotine promotes brain metastasis through activation of microglia

Because M2 microglia are abundantly infiltrated in brain metastatic lesions of current smokers, we examined the possibility that nicotine promotes brain metastasis by polarizing microglia to M2 microglia. We first examined the expression of nicotine receptors in microglia cells and in tumor cells and found that microglia expressed high levels of $\alpha4\beta2$, which is the most sensitive receptor of nicotine in the brain (Fig. 2 A). We also found that microglia expressed a significantly higher level of $\alpha4\beta2$ receptor than macrophage (Fig. S2 A). Moreover, the expression of $\alpha4\beta2$ receptor in microglia dramatically increased upon nicotine treatment (Fig. S2 A). We then examined the effect of nicotine on microglia polarization and tumor progression using the LL/2 mouse Lewis lung carcinoma model. The LL/2 cell is originated from the C57BL/6 mouse; however, this cell line can grow tumors in both C57BL/6 and BALB/c mice as reported previously (Janker et al., 2018; Kamei et al., 2009; Scholar et al., 1989). Therefore, we tested the effect of nicotine in both models. We intracardially inoculated luciferase-labeled LL/2 cells into both wild-type mice (C57BL/6 or BALB/c) followed by injecting nicotine (1 mg/kg) every 3 d until the end point. We found that nicotine significantly increased the incidence and growth of brain metastasis in both models (Fig. S2, B–D, for C57BL/6 model; Fig. 2 B and Fig. S2, E and F, for BALB/c model). On the other hand, nicotine did not promote bone metastasis (Fig. 2 B). The result of our immunohistochemical analysis for brain metastatic lesions revealed that high levels of activated microglial cells accumulated in the tumor mass in the nicotine-treated group (Fig. 2 C). Importantly, the majority of these microglia in the nicotine-treated mice were found to be M2 microglia (CD206$^+$/Iba1$^+$), and fewer M1 microglia (Iba1$^+$/F4/80$^+$) were identified in the brain lesions (Fig. 2 D and Fig. S2, G and H), suggesting that nicotine promoted microglia polarization to the M2 phenotype in the brain metastatic lesions. Infiltrated peripheral macrophages/microglia are known to modulate brain tumor progression (Bacha et al., 2018; Ellis et al., 2012). To define the exact role of macrophage and microglia on brain metastasis, we stained brain metastatic tumors with antibody against the macrophage marker CD45. We also examined the ratio of the number of microglia (CD45$^-$/Iba1$^+$) and peripheral macrophages (CD45$^+$/Iba1$^+$) in the brain metastatic lesions and found that macrophages comprised only 12–14% of CD45$^+$/Iba1$^+$ cells, and the number of macrophages was not altered between nicotine-treated and -untreated groups (Fig. S2 I). These results strongly suggest that nicotine promotes brain metastasis by skewing microglia to the M2 phenotype. To further validate this hypothesis, we examined the effect of depletion of "original" microglia by treating animals with the inhibitor for CSF 1 receptor (CSF1R), PLX3397. CSF1 signaling is necessary for microglia viability, and treating mice with PLX3397 has been previously shown to eliminate ∼99% of all microglia in the brain (Elmore et al., 2014). We therefore treated immune-competent wild-type mice with PLX3397 and transplanted them with LL/2 mouse lung cancer cells followed by nicotine treatment. To avoid a whole-body effect of PLX3397, the PLX3397 was locally injected into brain through intracranial injection 1 wk after the transplantation of LL/2 cells followed by nicotine treatment (Fig. S2 J). Strikingly, blocking microglia by PLX3397 significantly suppressed nicotine-related brain metastasis of lung cancer (Fig. 2, E–G), prolonged brain metastasis-free survival (Fig. 2 H), and repressed the nicotine-related M2 microglial polarization (Fig. 2, I and J) in the BALB/c mouse model. Similarly, PLX3397 suppressed nicotine-related brain metastasis and inhibited M2

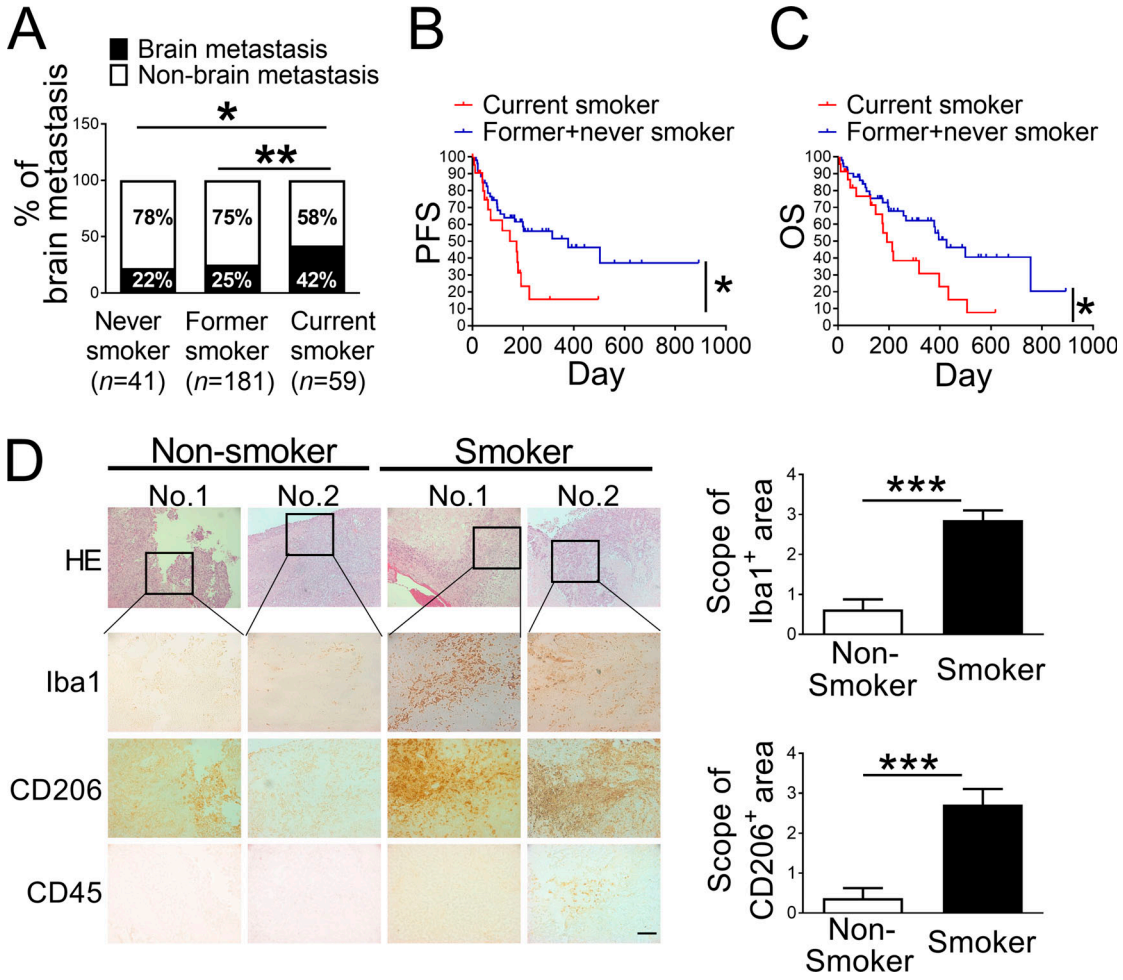

Figure 1. **Cigarette smoking increases incidence and mortality rate of lung cancer brain metastasis. (A)** Incidence of brain metastasis among 281 stage IV lung cancer patients composed of both current and noncurrent smokers at the time of diagnosis. All patients were admitted to Wake Forest Baptist Hospital. **(B and C)** Progression-free survival (PFS; B) and overall survival (OS; C) of patients with brain metastasis (n = 79) and with or without smoking history were examined by Kaplan–Meier analysis. **(D)** Representative images of immunohistochemical analysis for Iba1$^+$, CD206$^+$, and CD45$^+$ cells in the H&E-stained brain metastatic lesions of lung cancer patients who were current smokers (n = 7) and noncurrent smokers (n = 4). Scale bar, 100 µm. *, P < 0.05; **, P < 0.01; and ***, P < 0.001.

microglial polarization in the C57BL/6 mouse model (Fig. S2, K–N). We also treated nude mice with PLX3397 and transplanted them with H2030BrM cells via an intracardiac injection followed by nicotine treatment (Fig. S2, O–R). Nicotine-induced brain metastasis was significantly suppressed after PLX3397 treatment (Fig. S2, O–Q). The brain metastasis–free survival was also significantly prolonged by PLX3397 treatment (Fig. S2 R). PLX3397 treatment showed no detectable liver toxicity (Fig. S2 S). These results suggest that the nicotine-induced brain metastasis is indeed mediated by the effect of nicotine on microglia.

Nicotine skewed M2 microglial polarization

As shown in Fig. 2 D, the number of M2 microglia was increased after nicotine treatment, suggesting that nicotine promotes microglial polarization. To further investigate the effect of nicotine on microglia polarization, the microglial cells were treated with nicotine followed by measurement of expression of M1 and M2 markers. Our results showed that nicotine did not affect tumor cell proliferation (Fig. S2 T) at 1 µM concentration, but the same dose of nicotine significantly increased the mRNA expression of M2-related genes, *arginase-1* (*Arg1*), *arginase-2* (*Arg2*), and *CD204*, in both human and mouse microglial cells lines (Fig. 3, A and B) and mouse primary microglial cells (Fig. 3 C). Since STAT3 pathway is involved in M2 microglia (Qin et al., 2017), we examined the status of phospho-STAT3 and JAK expression in microglia with or without nicotine treatment, and found that nicotine treatment indeed enhanced the expressions of JAK/STAT3 (Fig. 3 D). We then treated the microglia with nicotine in the presence of STAT3 inhibitor (STATTIC) and found that inhibiting the STAT3 by STATTIC significantly suppressed the nicotine-induced STAT3 activation (Fig. 3 E). The *Arg1* gene is an M2 marker and is known to be regulated by STAT3 (Yi and Kim, 2017). We found that nicotine-induced up-regulation of the *Arg1* gene promoter was significantly suppressed by STATTIC treatment (Fig. 3 F). Moreover, inhibition of STAT3 reversed the nicotine-mediated suppression of Iba1$^+$/F4/80$^+$ (M1) and promotion of Iba1$^+$/CD206$^+$ cells (M2; Fig. 3, G and H). These results suggest that the nicotine promotes M2 microglial polarization via activation of the STAT3 pathway.

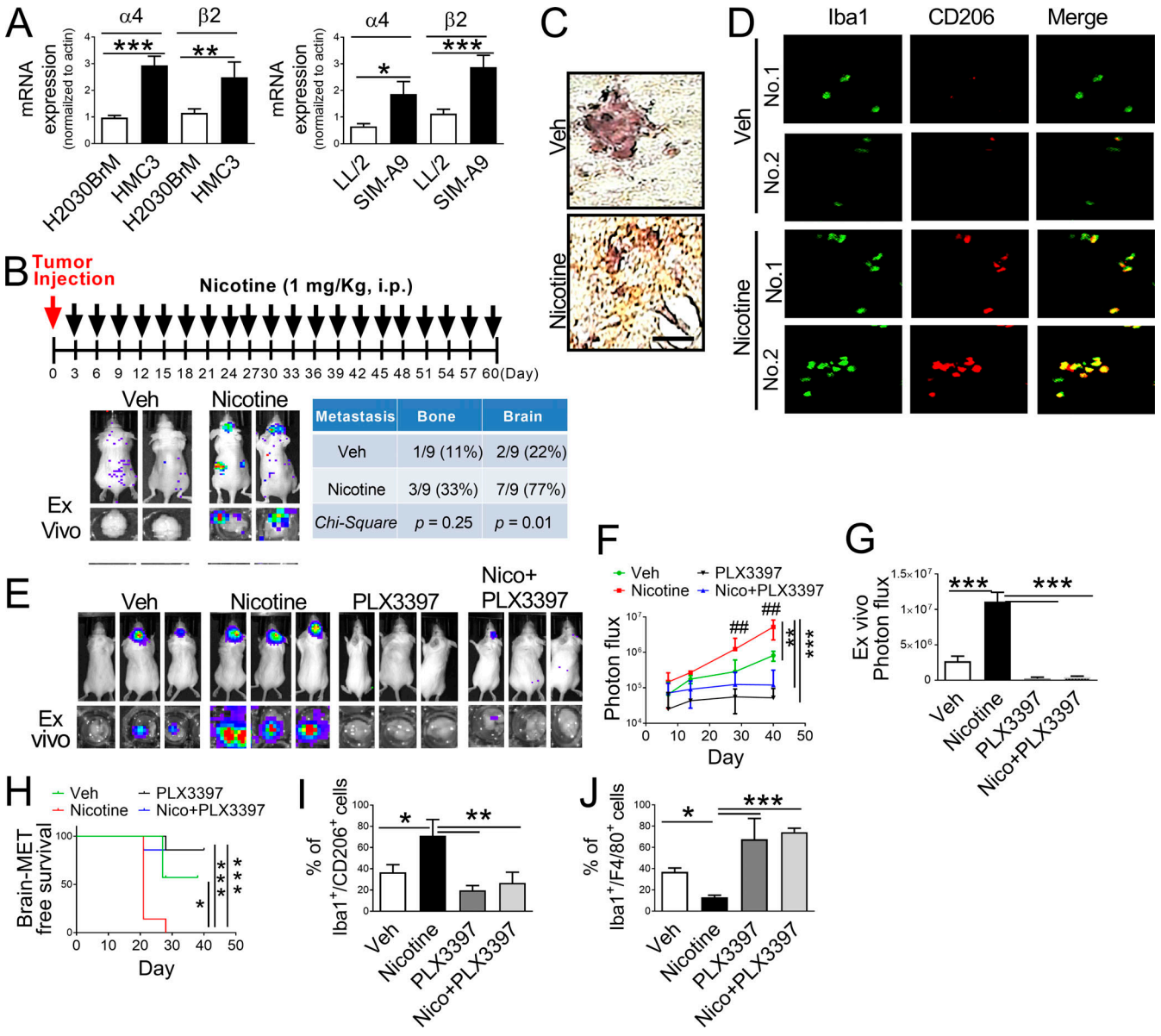

Figure 2. **Nicotine promotes brain metastasis by activating microglia in vivo. (A)** Expression of *α4β2* nicotine receptor on human microglia (HMC3), mouse microglia (SIM-A9), human lung cancer cells (H2030BrM), and mouse lung cancer cells (LL/2) were evaluated by qRT-PCR (n = 3/group). **(B)** LL/2 (5×10^4 cells) were intracardially injected into immune-competent BALB/c mice (n = 9). After 3 d of intracardiac transplantation of LL/2 cells, mice received nicotine treatment (1 mg/kg) by intraperitoneal injection every 3 d for 60 d. Upper panel: BLI images of brain metastatic lesions of representative mice from each experimental group (vehicle alone or nicotine treatment). Lower panel: total photon flux of ex vivo image of brain metastatic lesions was measured by BLI at the end point (day 60). Quantitative data of bone and brain metastasis of lung cancer are shown in the right panel. **(C)** At the end point, the brain sections from mice with or without treatment with nicotine were examined for $Iba1^+$ signal (brown) on microglia. Scale bar, 20 µm. **(D)** Representative images of immunohistochemical analysis for $CD206^+$ and $Iba1^+$ microglia in the metastatic brain lesions of mice that were treated with or without nicotine (n = 9/group). Scale bar, 100 µm. **(E)** Mouse lung cancer LL/2 cells were intracranially injected into wild-type BALB/c mice (n = 9/group) followed by administering PLX3397 by intracranial injection. Upper panels are BLI images of brain metastatic lesions of representative mice from each experimental group at day 40. Lower panels represent the total photon flux of ex vivo brain metastatic lesions as measured by BLI at the end point (day 40). **(F)** Quantitative data of in vivo brain metastasis of lung cancer (n = 9/group). **(G)** Ex vivo BLI signals in the brain at the end point (n = 9/group). **(H)** Kaplan–Meier analysis of brain metastasis–free survival was performed (n = 9/group). **(I and J)** Metastatic brain tumors in E were isolated from the brain and were examined by FACS for M2 (I) and M1 (J) microglial polarization (n = 4 or 5/group). The data are presented as the mean ± SD. *, P < 0.05; **, P < 0.01; and ***, P < 0.001 versus respective nicotine group. ##, P < 0.01 versus respective PLX3397 or Nico+PLX3397 group.

Nicotine-treated microglial cells promote tumor growth and stemness

To examine the effect of nicotine-induced M2 microglia on tumor progression, we treated lung cancer brain metastatic cells, H2030BrM and PC9BrM, with conditioned medium (CM) generated from human microglia that were treated with or without nicotine. We found that CM derived from nicotine-treated microglia significantly increased sphere formation (Fig. 4 A) and population of $ESA^+/CD44^+$ or aldehyde dehydrogenase ($ALDH^+$) cancer stem cells (CSCs; Fig. 4 B). The expression of stemness-inducing genes, *SOX2* and *NANOG*, was also significantly upregulated when the brain metastatic cells were treated with

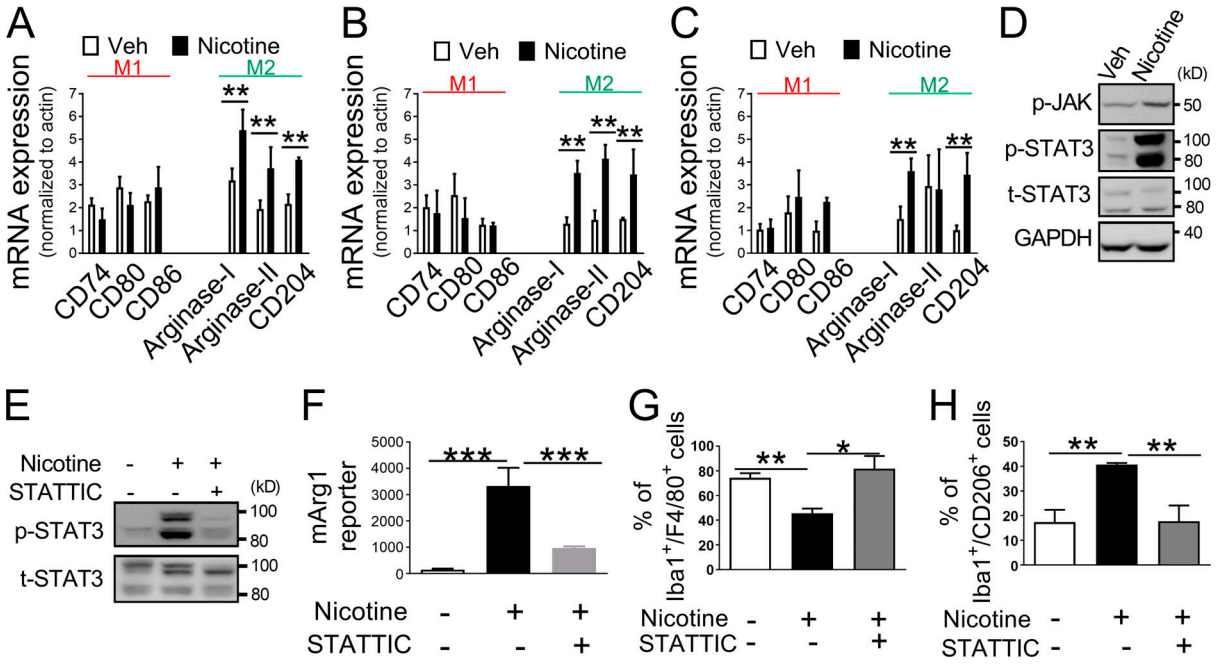

Figure 3. **Nicotine promotes M2 microglial polarization via STAT3 activation. (A–C)** Expressions of M1/M2 microglia markers were examined after the treatment of human microglia (HMC3) (A), mouse microglia (SIM-A9; B), and primary mouse microglia (C) with either vehicle or nicotine (1 µM). The value of qRT-PCR in each figure was normalized using actin as a control. The y axis indicates arbitrary unit (n = 3/group). **(D)** Human microglia (HMC3) were treated with or without nicotine (1 µM), and the expressions of JNK and STAT3 were examined by Western blot. **(E)** Human microglia (HMC3) were treated with or without nicotine and/or STATTIC (0.5 µM) for 24 h, and the expression of STAT3 was examined by Western blot. **(F)** Mouse microglia cells (SIM-A9) were treated with or without nicotine and/or STATTIC (0.5 µM) for 24 h followed by examining the luciferase-promoter activity of *Arg1* (M2; n = 4/group). **(G and H)** Mouse microglia (SIM-A9) were treated with or without nicotine (1 µM) and/or the STAT3 inhibitor (0.5 µM) for 24 h. Cells were then subjected to FACS analysis for analysis of Iba1$^+$/F4/80$^+$ (M1 cell; G) and Iba1$^+$/CD206$^+$ (M2 cell; H; n = 9/group). The data are presented as the mean ± SD. *, P < 0.05; **, P < 0.01; and ***, P < 0.001.

the CM of nicotine-treated microglia (Fig. 4, C and D). Furthermore, nicotine-treated microglial CM also promoted the colony-forming ability of both H2030BrM and PC9BrM cells (Fig. 4 E). We then sought to identify the factor(s) in CM that are responsible for the increase in stemness. We performed the cytokine array analysis (consisting of 99 factors) and found that nicotine significantly augmented the secretion of CCL20 and IGF-1 in the microglial CM (Fig. S3 A). The results of screening were verified using human microglial cells (Fig. S3 B). Furthermore, blocking STAT3 by STATTIC significantly suppressed nicotine-mediated up-regulation of CCL20 and IGF-1 (Fig. S3 B). We observed that microglia produced higher levels of IGF-1 and CCL20 than macrophage (Fig. S3 C). The expression of receptors of *IGF-1* and *CCL20* were significantly increased in H2030BrM cells after the treatment with CM of microglia that were exposed to nicotine (Fig. 4 F). We then treated lung cancer cells with recombinant CCL20 and IGF-1 and examined their effect on CSC properties. We found that both cytokines significantly enhanced the sphere formation (Fig. 4 G), ESA$^+$/CD44$^+$ CSC population (Fig. 4 H), and mRNA expression of CSC markers *SOX2* and *NANOG* (Fig. 4, I and J). In addition, IGF-1 and CCL20 significantly increased the colony-forming ability of brain metastatic lung cancer cells (Fig. 4 K). To understand the clinical relevance of these results, we used The Cancer Genome Atlas (TCGA) dataset and found that high expression of *CCL20* was associated with poor overall survival in lung cancer patients (Fig. S3 D); however, no such correlation was observed for the *IGF-1* gene (Fig. S3 E). Furthermore, expressions of both *CCL20* and its receptor, *CCR6*, were up-regulated in the primary tumor site of lung cancer patients compared with normal lung tissue in the same dataset (Fig. S3, F and G). Moreover, microglia expressed a higher level of *CCL20* mRNA than lung cancer cells, indicating that microglia are potentially major sources of *CCL20* in brain TME (Fig. S3, H and I). To examine whether CCL20 is involved in the growth-promoting effect of CM derived from nicotine-treated microglia, CCL20 was depleted in the CM using CCL20 neutralizing antibody. Our result indicates that depletion of CCL20 significantly suppressed the generation of CSC by nicotine-treated CM (Fig. 4 L). To further validate our results, we examined the levels of CCL20 in brain and serum of the nicotine-treated mice represented in Fig. 2 E and found that CCL20 indeed increased in the brain and serum of nicotine-treated animals (Fig. 4, M and N). In contrast, depletion of microglia by PLX3397 significantly suppressed the levels of nicotine-induced CCL20 in brain and serum of nicotine-treated animals (Fig. 4, M and N). Furthermore, consistent with our in vivo results, we found that the serum level of CCL20 was significantly higher in lung cancer patients who were current smokers compared with noncurrent smokers (Fig. 4 O).

We also examined the direct effect of nicotine on cell growth by treating the human lung cancer brain metastatic cells, H2030BrM, with nicotine alone or with nicotine-treated

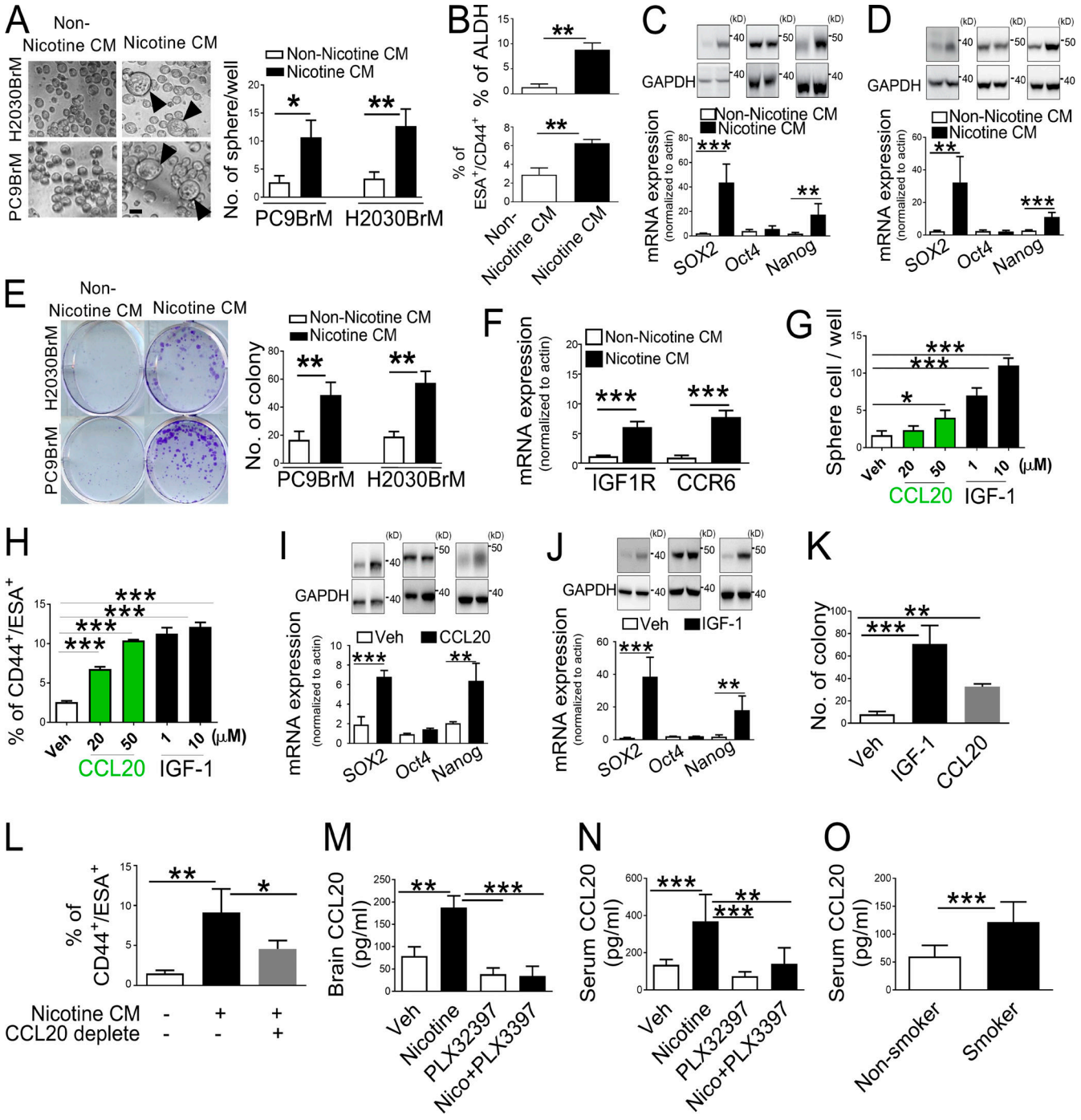

Figure 4. **Nicotine-mediated microglial polarization promotes tumor stemness. (A)** Effect of human microglial cells (HMC3) treated with or without nicotine (1 μM), and collection of CM. Brain metastatic lung cancer cells (H2030BrM and PC9BrM) were treated with the non-nicotine and nicotine CM for 24 h, and their sphere-forming ability was measured. Left panel: representative images. Arrowheads indicate sphere formation. Right panel: quantification of number of spheres. Non-nicotine or nicotine CM: microglia cells were treated with PBS or nicotine (1 μM) for 24 h, and they were washed with PBS and incubated in the fresh DMEM/F12 medium supplemented with 2% FBS for 24 h (n = 4/group). Scale bar, 10 μm. **(B)** Effect of the human microglial CM on CSC markers, ESA$^+$/CD44$^+$, and ALDH activity were examined using FACS (n = 4/group). **(C and D)** Expressions of stemness genes in H2030BrM (C) and in PC9BrM cells (D) were examined after the treatment with or without nicotine-derived human microglial CM by qRT-PCR (n = 6/group). **(E)** Colony-forming abilities of H2030BrM and PC9BrM cells were measured in the presence or absence of the CM derived from nicotine-treated human microglia. Left panel: representative images. Right panel: quantification of number of colonies (n = 4/group). **(F)** Expressions of *IGF-1* and *CCL20* receptors in H2030BrM cells were examined after the treatment of cells with or without nicotine-derived human microglial CM by qRT-PCR (n = 4/group). **(G)** Effect of recombinant proteins, CCL20 and IGF-1, on sphere formation ability of H2030BrM was measured (n = 3/group). **(H)** H2030BrM cells were treated with CCL20 or IGF-1 for 24 h followed by measuring the ESA$^+$/CD44$^+$ stem cell population by FACS (n = 4/group). **(I and J)** H2030BrM cells were treated with or without 20 μM of CCL20 (I) or 1 μM of IGF-1 (J) for 24 h, and the expressions of stemness genes were examined by qRT-PCR and Western blot (n = 4/group). **(K)** Colony-forming assay was performed for the same set of samples as in G and H (n = 4/group). **(L)** Human microglia were treated with or without nicotine (1 μM) for 24 h, and their CM was prepared. The CM was then

added with anti-CCL20 antibody to deplete CCL20. H2030BrM cells were then treated with the CCL20-depleted CM followed by assaying the ESA$^+$/CD44$^+$ stem cell population by FACS (n = 4/group). **(M and N)** Metastatic lesions in the brain and serum were prepared from the mice used in Fig. 2 E. The protein expression of CCL20 in the brain (M) and in the serum (N) in each group was measured by ELISA (n = 6/group). **(O)** The protein expression of CCL20 in the serum of lung cancer patients with or without smoking history were measured by ELISA (n = 10/group). The data are presented as the mean ± SD. *, P < 0.05; **, P < 0.01; and ***, P < 0.001.

microglial CM. Although colony-forming ability increased in both groups (Fig. S3 J), the CSC population and expression of stem cell markers were significantly elevated only in cells treated with the nicotine-treated microglial CM (Fig. S3, K and L). Consistent with these results, treating the mouse lung cancer cell, LL/2, with CM derived from nicotine-treated mouse microglia significantly increased the levels of CSCs (Fig. S3 M) and promoted the colony-forming ability (Fig. S3 N) and tumor cell viability (Fig. S3 O). We also examined whether nicotine-induced brain metastasis is mediated via M2 microglial polarization by STAT3 activation. We blocked the M2 polarization of microglia by STATTIC and examined the expression of *IGF-1* and *CCL20* by quantitative real-time PCR (qRT-PCR). We found that the nicotine treatment significantly up-regulated the *IGF-1* and *CCL20*, while STATTIC reversed the effect (Fig. S3, P and Q). The CM was then added to the culture of LL/2 cells. We found that CM derived from microglia that were treated with both nicotine and STATTIC significantly suppressed CSC population (Fig. S3 R) and tumor cell viability (Fig. S3 S).

Nicotine suppresses innate immune function of microglia

Microglia are known to exhibit phagocytic activity against brain tumor cells, like macrophages (Hutter et al., 2019). However, to escape from microglia-mediated phagocytosis, tumor cells express CD47 on their cell surface, which activates so-called "do not eat me" signaling. To investigate if nicotine affects this immune function of microglia, we measured the expression of signal-regulatory protein α (SIRPα) on microglia and CD47 on tumor cells. We found that the mRNA and protein expression of SIRPα were up-regulated in human microglia after nicotine treatment (Fig. 5 A). We also found that nicotine significantly increased the mRNA and protein expression of CD47 in both H2030BrM and PC9BrM cells (Fig. 5 B). Importantly, the expression of CD47 is up-regulated in brain metastasis of lung cancer patients with smoking history (Fig. 5 C). We then examined the effect of nicotine on phagocytic ability of microglia. We prelabeled H2030BrM cells with the fluorochrome-PKH26, a red-fluorescent vital dye that binds tightly to cell membranes (Munn and Cheung, 1990). The labeled cells were incubated with microglia that were treated with or without nicotine. We found that the size of PKH26$^+$ tumor cells and microglia cells was similar at 0 h in the co-culture (Fig. 5 D). However, after 24 h of incubation, the small and irregular shape of PKH26$^+$ cells was accumulated in the microglia. This result suggests that tumor cells were rapidly degraded by nicotine-treated microglia through phagocytosis. As shown in Fig. 5, D and F, both human and mouse microglial cells showed strong phagocytic activities toward the H2030BrM and LL/2 cells. Importantly, this phagocytic ability was greatly compromised in the presence of nicotine (Fig. 5, E and G). Blocking STAT3 signaling by STATTIC treatment suppressed nicotine-mediated down-regulation of phagocytic ability of microglia (Fig. 5 E). We also examined the expression of SIRPα in microglia of the nicotine-treated mouse brain represented in Fig. 2 E and found that the CD47 and SIRPα expression were strongly elevated in the brain of mice treated with nicotine (Fig. 5, H–J). These results suggest that nicotine promotes M1/M2 conversion and suppresses the innate immune function of microglia, which promotes brain metastasis progression.

PTL suppresses nicotine-induced M2 microglia polarization and enhances their phagocytic ability

Our results strongly suggest that blocking M2 polarization of microglia may be an effective therapeutic approach for brain metastasis. Therefore, we screened a natural compound library to identify compounds that block M2 macrophage polarization using an Arg1 promoter reporter system. We screened a total of 103 compounds that are known to be blood–brain barrier (BBB) permeable. As shown in Fig. S4 and Fig. 6 A, we identified three compounds (>15-fold change, P < 0.001) that effectively suppressed the nicotine-induced activation of *Arg1* promoter at a concentration of 1 μM. We selected the top compound, PTL, which suppressed the *Arg1* promoter activity by >20-fold, for further study (Fig. 6 A). PTL is an abundant sesquiterpene lactone found in the medicinal herb Feverfew (*Tanacetum parthenium*). It has been used to treat inflammation and headache for centuries in Europe (Liu et al., 2018). To confirm the suppressive effect of PTL on nicotine-induced M2 microglial polarization, microglia were treated with nicotine in the presence or absence of PTL (Fig. S5 A), and expressions of M1 and M2 markers were examined. We found that PTL significantly decreased the nicotine-mediated M2 polarization of microglia (Fig. 6 B). Furthermore, the nicotine-mediated reduction of Iba1$^+$/CD11b$^+$ cells (M1) and elevation of Iba1$^+$/CD206$^+$ cells (M2) were significantly reversed by PTL (Fig. 6 C). Previous studies have shown that PTL modulated the JAK2/STAT3 signaling in response to cytokine stimulations (Liu et al., 2018; Sobota et al., 2000). We indeed found that PTL suppressed the nicotine-induced JAK2/STAT3 activation (Fig. 6 D), suggesting that PTL blocks the nicotine-induced M2 microglial polarization by targeting STAT3. Furthermore, the nicotine-induced suppression of phagocytic ability of microglia was restored when cells were treated with PTL (Fig. 6 E). The H2030BrM cells were treated with CM of microglia that were exposed to nicotine only or nicotine plus PTL. We found that the ESA$^+$/CD44$^+$ CSCs (Fig. 6 F) and colony-forming ability (Fig. 6 G) were significantly suppressed by CM of microglia treated with nicotine plus PTL. We also examined the mRNA expression of *CCL20* and found that the nicotine-mediated secretion of CCL20 was down-regulated by the PTL treatment (Fig. 6 H). Next, to investigate the effect of PTL on

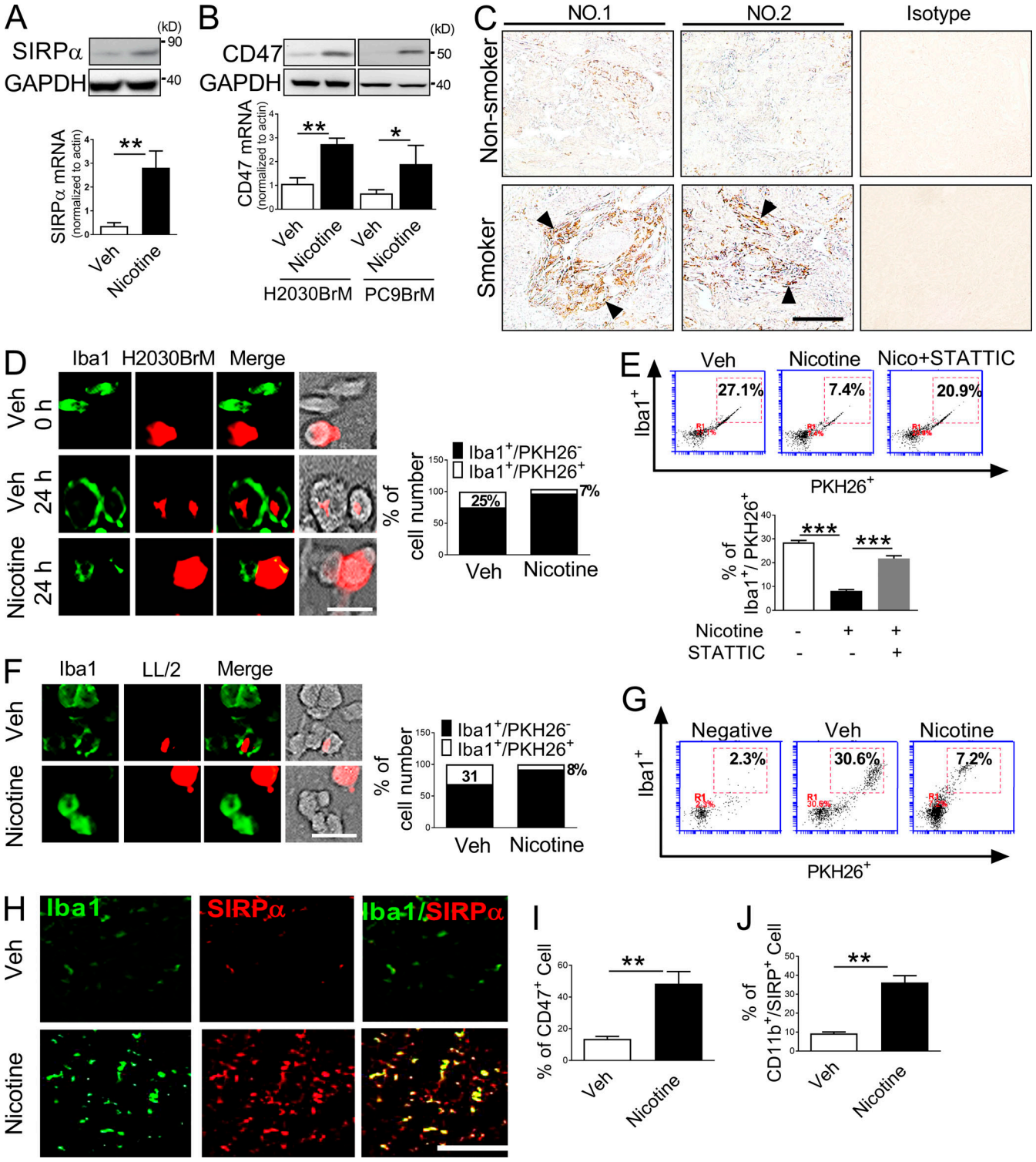

Figure 5. **Nicotine suppresses innate anti-tumor immune function of microglia. (A)** Human microglia cells (HMC3) were treated with or without nicotine (1 μM) for 24 h, and the expression of SIRPα was examined by qRT-PCR and Western blot (n = 4/group). **(B)** H2030BrM and PC9BrM cells were treated with or without nicotine (1 μM) for 24 h, and the expression of CD47 was examined by qRT-PCR and Western blot (n = 4/group). **(C)** Representative images of immunohistochemical analysis for CD47⁺ cells in the metastatic brain lesions of lung cancer patients with or without smoking history. Arrows indicate CD47⁺ cells. Non-smoker (n = 4) and smoker (n = 7). Scale bar, 50 μm. **(D)** Phagocytic activities of HMC3 human microglial cells (green) with or without nicotine treatment were examined using PKH26-labeled H2030BrM cells (red). Both cells were incubated together for 0 or 24 h and photographed (left panels), and the number of microglia that phagocytosed tumor cells was counted to quantify microglial phagocytic activity as shown in the right panel (n = 4/group). Scale bar, 10 μm. **(E)** A parallel set of cells in D was analyzed by FACS to quantify phagocytic abilities of microglia after nicotine or STATTIC treatment. Upper panels: representative FACS data. Lower panel: statistical analysis of the FACS data (n = 4/group). **(F)** Mouse microglia (SIM-A9; green) were incubated with PKH26-labeled LL/2 mouse lung cancer cells (red) for 24 h. They were then photographed under a fluorescent microscope (n = 4/group). Scale bar, 100 μm.

(G) Phagocytic abilities of microglia with or without nicotine treatment were examined by incubating mouse microglia with PKH26-labeled LL/2 mouse lung cancer cells for 24 h, followed by analysis of the cells by FACS (n = 4). **(H)** The metastatic lesions in the brain of mice in Fig. 2 E were sectioned, and they were subjected to immunohistochemical analysis for SIRPα and Iba1. Representative immunohistochemistry images of the microglia are shown (n = 9/group). Scale bar, 100 µm. **(I and J)** The metastatic lesions in the brain of mice in Fig. 2 E were subjected to FACS analysis for $CD47^+$ tumor cell (I) and $SIRP\alpha/CD11b^+$ (J) microglia cells (n = 9/group). The data are presented as the mean ± SD. *, P < 0.05; **, P < 0.01; and ***, P < 0.001.

nicotine-related brain metastasis in vivo, wild-type mice (C57BL/6 and BALB/c) were transplanted with LL/2 mouse lung cancer cells followed by administering nicotine (1 mg/kg) only or nicotine plus PTL (1 mg/kg) via an intraperitoneal injection. As shown in Fig. 6, I-K (BALB/c) and Fig. S5, B and C (C57BL/6), PTL treatment significantly suppressed nicotine-mediated brain metastasis and prolonged the brain metastasis–free survival (Fig. 6 L). To examine whether the PTL treatment also reverses microglia polarization in the brains of these mice, we performed flow cytometry (FACS) analysis of mouse brain and stained brain sections for M1 and M2 markers. A significant increase in $Iba1^+/F4/80^+$ (M1 marker) and decrease in $Iba1^+/CD206^+$ (M2 marker) were observed in brain microglia of PTL-treated mice (Fig. 6, M and N; and Fig. S5, D and E). To validate our results in human cell line, we used the xenograft model of H2030BrM cell and tested the efficacy of PTL. As shown in Fig. S5, F–K, PTL significantly suppressed the nicotine-induced brain metastasis and M2 microglia polarization. PTL treatment did not affect body weight of mice and showed no detectable liver toxicity (Fig. S5 L). We also examined the direct effect of PTL on cell viability and CSC population in vitro (Fig. S5 M). Our results showed that PTL suppressed the abundance of $CD44^+/ESA^+$ CSC and cell viability at the concentration of 10–20 µM, but not at 1 µM, which is the dose used throughout our in vitro experiments (Fig. S5, N and O), indicating that the anti-tumor effect of PTL is not mediated by direct cytotoxic effect, and it is rather mediated by the effect on microglia. Furthermore, PTL significantly suppressed stemness promoting effect of nicotine on microglia (Fig. S5 P) and the expression of stemness-related genes (Fig. S5, Q and R). These results suggest that PTL suppresses nicotine-related brain metastasis of lung cancer by skewing polarity of M1 microglia and up-regulating their phagocytic ability.

Discussion

The incidence of brain metastasis among lung cancer patients is 10–36% (Bacha et al., 2018; Barnholtz-Sloan et al., 2004; Schouten et al., 2002), although these data are considered to be underestimated (Bacha et al., 2018; Schouten et al., 2002). The majority of the lung cancer patients are diagnosed with advanced stage disease, most with stage IV cancer. More than 90% of lung cancer deaths are attributed directly to the metastatic disease and include those brain metastases (Ali et al., 2013; Kakusa et al., 2018). Cigarette smoking is a major risk factor for lung cancer (Lee et al., 2012), and our previous study showed a negative impact of smoking on lung cancer brain metastasis (Shenker et al., 2017). In the present study, we have found a significantly higher incidence of brain metastasis among current smokers with stage IV lung cancer.

Nicotine is not a carcinogen, but it causes addiction by activating nAch receptor, which is abundantly expressed by various brain cells including microglia. Direct tumor promoting effects of nicotine have been previously reported (Schaal and Chellappan, 2014; Sun et al., 2017; Wang et al., 2017; Yoneyama et al., 2016); however, how nicotine promotes tumor by activating TME is still poorly understood. The current report is the first to show the critical impact of nicotine on brain TME to promote brain metastasis by skewing microglia to M2 phenotype and suppressing their role in innate immunity. Our results indicate that the phenotypic conversion of microglia by nicotine is mediated through the nAch receptor–STAT3 pathway, and that inhibition of STAT3 blocked the M2 conversion, suppressed the secretion of pro-tumor M2 cytokines, and reactivated their phagocytic activity toward tumor cells (Fig. 6 O).

Previous studies showed that microglial cells and macrophages in the brain are derived from two different sources, parenchymal resident microglia and monocytes/macrophages that enter the brain from the bone marrow (Wu and Watabe, 2017). Although microglia and macrophage cells show similarity in their surface markers and physiological functions, recent studies have demonstrated that microglia and macrophages are two distinct myeloid populations with different developmental origins (Gomez Perdiguero et al., 2015; Prinz and Priller, 2014; Schulz et al., 2012). Microglial cells originate from erythromyeloid progenitors that begin on embryonic day (E) 7.5–E8.0. in the blood islands of the yolk sac. Until E9.5, erythromyeloid progenitors migrate to the developing central nervous system and mature into microglia (Gomez Perdiguero et al., 2015; Prinz and Priller, 2014; Schulz et al., 2012). These early microglial cells reside in the brain throughout life and are thought to sustain the local microglial population. In contrast, macrophages originate from the hematopoietic stem cells that start in the aorta–gonad–mesonephros region at E10.5. and then in the fetal liver at E12.5. After the postnatal stage, macrophages are produced from monocytes in the bone marrow (Gomez Perdiguero et al., 2015; Prinz and Priller, 2014; Schulz et al., 2012). Furthermore, recent studies demonstrated that microglial cells and macrophage have distinct and specific surface antigens (Feng et al., 2015). Studies on CX3CR1 ($^+$/GFP)/CCR2 ($^+$/RFP) knock-in fluorescent protein reporter mice revealed that microglial cells are $CX3CR1^+/CCR2^-/CD45^-$, while the macrophages are $CX3CR1^-/CCR2^+/CD45^+$ (Feng et al., 2015), strongly supporting the notion that microglial cells and macrophages are from different populations and they can be distinguished. Badie and Schartner performed flow cytometric analysis and characterized the distribution of microglial cells and macrophages in experimental gliomas and found that microglial cells ($CD11b/c^{high}$, $CD45^{low}$), mainly present at the site of tumor or tumor periphery, accounted for 13–34% of the tumor mass. In contrast, macrophages ($CD11b/c^{high}$, $CD45^{high}$) were less prominent within the tumors or the tumor periphery and accounted for just

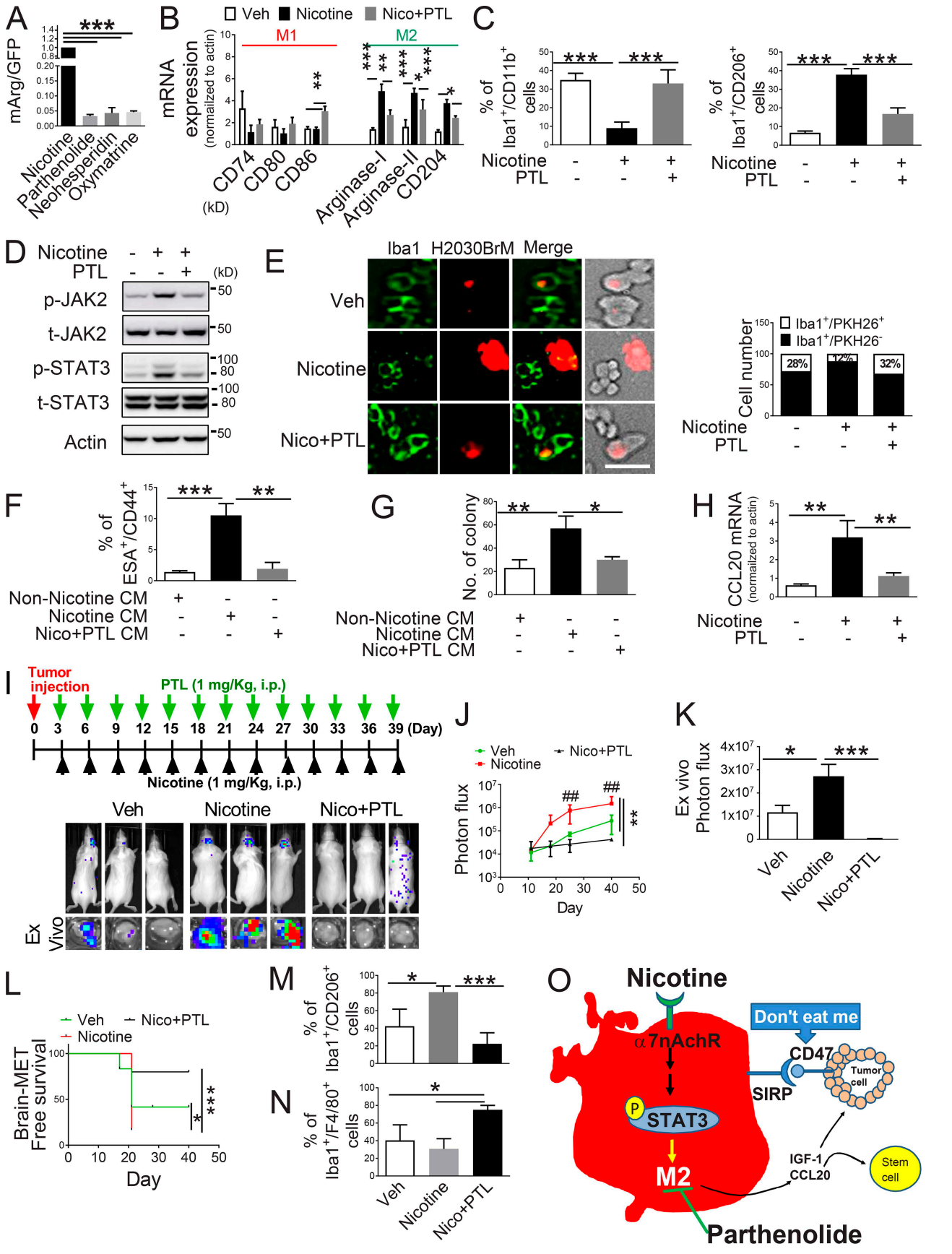

Figure 6. **PTL suppresses brain tumor progression by blocking nicotine-induced M2 microglia polarization. (A)** Human microglia cells (HMC3) with the Arg1 reporter plasmid were cultured in the presence or absence of compounds that were identified as the top three most effective inhibitors for Arg1 during our

initial screening (see Materials and methods). After 48 h of incubation, luciferase reporter activity was measured (n = 4/group). **(B)** Expression of surface markers of M1/M2 microglia was examined by qRT-PCR after microglial cells were treated with or without nicotine plus PTL (n = 4/group). **(C)** The same set of samples in B was evaluated for quantification of Iba1$^+$/CD11b$^+$ (M1) cells and Iba1$^+$/CD206$^+$ (M2) cells by FACS (n = 4/group). **(D)** The same set of samples in C was examined for quantification of the protein expression of JAK2 and STAT3 by Western blot. **(E)** Human microglial (HMC3) cells (green) with or without nicotine treatment (1 µM) in the presence or absence of PTL (1 µM) were incubated with PKH26-labeled H2030BrM cells (red) for 24 h and photographed (left panels), followed by measurement of the microglial phagocytic activity (right panel; n = 4/group). Scale bar, 10 µm. **(F)** CM was prepared from human microglia (HMC3) treated with or without nicotine and PTL. The CM was added to the culture of H2030BrM, and cells were incubated for 48 h followed by evaluation of CSC population by FACS. Non-nicotine, nicotine, or Nico+PTL CM: microglia were treated with PBS, nicotine, or nicotine plus PTL for 24 h. They were then washed twice with PBS and incubated in the fresh DMEM/F12 medium supplemented with 2% FBS for a further 24 h (n = 4/group). **(G)** For the same set of samples as F, colony-forming ability was also measured (n = 4/group). **(H)** Human microglia were treated with or without nicotine (1 µM) in the presence or absence of PTL for 24 h, followed by assessment of the expression of *CCL20* by qRT-PCR (n = 4/group). **(I)** The mouse lung cancer cells, LL/2, were intracardially injected into wild-type BALB/c mice. After 3 d of intracranial transplantation of LL/2 cells, mice received nicotine (1 mg/kg) plus PTL (1 mg/kg) by an intraperitoneal injection every 3 d for 40 d. Upper panel: BLI images of representative mice from each experimental group at day 40. Lower panel: total photon flux of ex vivo brain metastatic lesions was measured by BLI at the endpoint (day 40; n = 9/group). **(J)** Quantitative data of BLI in the brain regions are shown (n = 9/group). **(K)** Ex vivo signals in the whole brains at the end point were quantified. **(L)** The Kaplan–Meier analysis of brain metastasis–free survival was performed (n = 9/group). **(M and N)** Metastatic brain tumors in I were isolated from the brain and were examined by FACS for M2 (M) and M1 (N) microglial polarization (n = 9/group). **(O)** A proposed model illustrating a nicotine-induced brain metastasis (n = 9/group). The data are presented as the mean ± SD. *, $P < 0.05$; **, $P < 0.01$; and ***, $P < 0.001$.

4.2–12% of the tumor mass (Badie and Schartner, 2000). These results also suggest that microglial cells play a key role in mediating brain tumor progression.

We have also found that nicotine dramatically increased the mRNA expression of α4β2 receptor on microglia cell compared with macrophage. These results suggest that microglia is more responsive to nicotine compared with macrophage, resulting in increase in the incidence of brain metastasis. Furthermore, it was reported that the numbers of macrophage/microglia were significantly higher in the central nervous system than in the peripheral system after injury (Leskovar et al., 2000). In addition, the peak concentrations of three cytokines, TNFα, IL-1, and IL-6, appeared earlier and were significantly higher in the injured central nervous system than peripheral system (Leskovar et al., 2000), suggesting differences in the reparative responses of macrophage/microglia in the PNS and central nervous system to injury.

In this study, we showed that blocking microglia CSF1R by PLX3397 significantly suppressed nicotine-mediated brain metastasis, suggesting that cancer cells lose growth support function from M2 microglia. Previous studies showed that PLX3397 reprogrammed tumor-infiltrating macrophages, enhanced antigen presentation (Zhu et al., 2014), and suppressed TAM infiltration in the tumor (Butowski et al., 2016; Cannarile et al., 2017; Cuccarese et al., 2017). We also found that PLX3397 skewed the population of microglia/macrophage to M1 phenotype. Therefore, while blocking the proliferation of microglia/macrophage, PLX3397 also promotes the residual microglia's innate immune function to tumor cells. Our results indicate that nicotine increased the secretion of IGF-1 and CCL20 in the CM of microglial cells. IGF-1 is known to enhance tumor cell survival and proliferation via activation of the PI3K-Akt signaling (Park et al., 2016; Zhu et al., 2011). However, the role of CCL20 on tumor progression has not yet been well defined. CCL20 is a critical chemoattractant responsible for the recruitment of inflammatory immune cells (Nandi et al., 2014). The expression of CCL20 has been shown to be overexpressed in a variety of tumors including lung cancer (Liu et al., 2016; Wang et al., 2015, 2016). In pancreatic cancer, CCL20 has been found to be overexpressed in metastatic tumor tissues (Liu et al., 2016). It was reported to promote epithelial–mesenchymal transition and invasive ability of tumor cells by activating the MAPK and PI3K pathways and matrix metallopeptidase signaling (Marsigliante et al., 2016; Wang et al., 2016). Previous studies showed that CCL20 promotes cell proliferation through activation of MAPK pathway (Lu et al., 2017) and up-regulating transcription of c-Fos and c-Myc. Others have shown that CCL20 enhanced the chemotherapy resistance of triple-negative breast cancer by promoting ALDH$^+$ population of breast cancer cells through PKCζ- and p38 MAPK-mediated NF-κB activation (Chen et al., 2018). We found that stem cell genes *NANOG* and *SOX2* were up-regulated in CCL20-treated cells, suggesting that CCL20 promoted the stemness of lung cancer brain metastatic cells via *NANOG/SOX2*. One of the major sources of CCL20 is a tumor-associated macrophage, especially M2 macrophage (Liu et al., 2016). In this study, we found that nicotine strongly promoted phenotypic conversion of microglia to M2 and enhanced secretion of CCL20 to stimulate tumor cell growth and cancer cell stemness. The depletion of microglia in our animal model significantly reversed the effect of nicotine on brain metastasis. Furthermore, we showed that the effect of CCL20 on tumor stem cell was mediated by up-regulation of *SOX2* and *NANOG* genes. These results suggest that CCL20 may serve as a novel therapeutic target and biomarker for brain metastasis of lung cancer.

SIRPα is expressed predominantly in myeloid and neuronal cells (Adams et al., 1998; Kharitonenkov et al., 1997). Normal cells express CD47 that interacts with SIRPα on macrophage/microglia to suppress their phagocytic activity. Several studies have shown that the expression of SIRPα is also associated with polarization of microglia/macrophage (Pan et al., 2013). Furthermore, knockdown of SIRPα in macrophages increased the production of M1 cytokines in the tumor environment (Pan et al., 2013). Blocking SIRPα also triggered the Akt survival signal in macrophages and enhanced macrophage migratory activities toward tumors (Pan et al., 2013), suggesting that SIRPα also affects microglia's function. In this study, we found that the nicotine increased the expression of SIRPα on microglia, while nicotine also promoted the expression of CD47 on the tumor

cells, resulting in suppression of phagocytic ability of microglia. There are two possible mechanisms that are involved in the anti-tumor effect of microglia. One is direct internalization of tumor cells into the lysosome of microglia by phagocytosis. The other possibility is that tumor cells are first killed by cytotoxic factors released by microglia followed by phagocytosis of the apoptotic debris by microglia. In addition, it is noteworthy that the CD47-SIRPα signal was previously found to modulate T cell differentiation and regulate T cell priming to the tumor site (Liu et al., 2015b; Zhang and Petro, 1996). Therefore, the CD47-SIRPα signal that was activated by nicotine plays a pivotal role in modulating anti-tumor innate as well as adaptive immune responses in TME.

By screening a BBB permeable natural compound library, we identified PTL as a potent inhibitor for nicotine-induced M2 conversion of microglia. PTL is an abundant sesquiterpene lactone found in the medicinal herb Feverfew (*T. parthenium*). It has been used for centuries as a traditional medicine to treat arthritis, fever, and headache (Liu et al., 2015a; Rummel et al., 2011). PTL was also previously shown to exhibit direct tumor suppressive activity (Talib and Al Kury, 2018) by modulating multiple pathways, including p53, vascular endothelial growth factor (Talib and Al Kury, 2018), B-Raf/MAPK/Erk (Lin et al., 2017), and STAT3 pathways (Carlisi et al., 2011; Skoumal et al., 2011; Song et al., 2014). However, these direct tumor cytotoxic effects mediated by PTL require a relatively high dose, typically >10 μM. In this study, we found that sub-micromolar dose (<1 μM) of PTL effectively suppressed nicotine-induced polarization of microglia to M2 phenotype and enhanced its M1 phenotype. On the other hand, the low concentration (1 μM) of PTL did not affect the population of CSC or tumor cell growth, which strongly suggests that the anti-tumor effect of PTL on nicotine-promoted brain metastasis shown in our study is mediated via modulation of microglial function and not by direct effect of PTL on tumor cells. Importantly, PTL was shown to be able to cross the BBB due to high membrane permeability (Könczöl et al., 2013). Considering the inhibitory effect of PTL on nicotine-induced microglial activation and their minimum toxicity at the effective dose, PTL could be used for the prevention and treatment of brain metastasis, particularly for patients with past and current smoking history.

Nicotine is highly addictive and considered as the major obstacle for smoking cessation (Henningfield et al., 1991). Unfortunately, many cancer patients have difficulty in quitting smoking even after their diagnosis due to nicotine addiction. E-cigarette, nicotine patch, and nicotine gum are nicotine replacement therapies for smoking cessation used by these patients (Hartmann-Boyce et al., 2018; Stead et al., 2012). Although nicotine, per se, is not a carcinogen, many reports document its tumor-promoting effects (Li et al., 2017; Schaal and Chellappan, 2014; Schaal et al., 2018) as well as its pro-inflammatory effect, which suppresses the phagocytosis ability of the alveolar macrophages (Scott et al., 2018). Considering our results that clearly demonstrated profound and long-term effects of nicotine on brain metastasis progression, extra caution should be paid in the use of nicotine for smoking cessation.

Materials and methods

Human subjects

We used a cohort of patients with a diagnosis of nonsmall cell lung cancer with or without brain metastases treated at Wake Forest Baptist Comprehensive Cancer Center between May 2015 and April 2018. We collected a total of 281 stage IV nonsmall cell lung cancer patients with or without a history of smoking. Among them, 79 patients were diagnosed with brain metastasis. 59 patients were current smokers at the time of diagnosis and treatment. We defined the "never smokers" (n = 44) as those who have no smoking history and those who had smoked <10 pack/year but stopped smoking. The "former smokers" (n = 181) are defined as those who smoked >10 pack/year but quit smoking in the past. Patient characteristics included histology status, smoking history, pack/years, progression status, and date of death. Patient information about age, gender, cancer type, and smoking status are described in Fig. S1. All samples used in this study were obtained under the approval of the institutional review boards of Wake Forest School of Medicine Institutional and Wake Forest Baptist Comprehensive Cancer Center. Written informed consent was obtained from all participants.

Cell culture and reagents

Human lung cancer cell lines, H2030BrM and PC9BrM, were kind gifts from J. Massagué (Memorial Sloan-Kettering Cancer Center, New York, NY). H2030BrM and PC9BrM cell lines were authenticated by using GenePrint 10 STR System (Promega, B9510). SIM-A9 was obtained from Kumi Nagamoto-Combs, through Kerafast.com. HMC3 and LL/2 cells were purchased from American Type Culture Collection (ATCC) and were authenticated by ATCC. The H2030BrM and PC9BrM were cultured in RPMI supplemented with 10% FBS, streptomycin (100 mg/ml), and penicillin (100 U/ml). LL/2 cells were cultured in DMEM medium supplemented with 10% FBS. SIM-A9 and HMC3 were cultured in DMEM/F12 medium supplemented with 5% FBS. All cells were grown at 37°C under 5% CO_2. All cell lines were obtained between 2010 and 2016, and they were ensured to be negative of mycoplasma. The HMC3 and SIM-A9 cells were seeded in a 10-cm dish. After reaching 70% confluence, cells were incubated with or without 1 μM nicotine in DMEM/F12 medium supplemented with 2% FBS or in medium containing nicotine plus the STAT3 inhibitor STATTIC (0.5 μM). After 24 h, cells were washed twice with PBS and then incubated in the fresh DMEM/F12 medium supplemented with 2% FBS for 24 h. The CM harvested from the cell culture were centrifuged at 300 *g* for 10 min to remove the cells and stored at −80°C. To investigate the effect of nicotine-derived CM on tumor progression, we harvested CM from microglial cells that were treated with or without nicotine, followed by treatment of tumor cells with the CM. All cell lines were tested by using universal mycoplasma detection kit (ATCC, 30-1012k, lot 70008746).

Animal models

Animals were treated in accordance with the U.S. National Institutes of Health Animal Protection Guidelines, and the protocol was approved by the Wake Forest Baptist Health Institutional

Animal Care and Use Committee. Female nude, BALB/c, and C57BL/6 mice of 5–6 wk of age were used. The mice were housed (four to five per cage) at a stable temperature (24 ± 1°C), in a 12-h light/dark cycle, and with unrestricted access to food and water. Several studies showed that human lung adenocarcinomas cell H2030BrM and mouse Lewis lung carcinoma cell LL/2 exhibited their highly metastatic abilities in the nude, C57BL/6, and BALB/c mice, respectively (Chen et al., 2016; Janker et al., 2018; Kamei et al., 2009; Malladi et al., 2016; Nguyen et al., 2009; Scholar et al., 1989). Actively growing luciferase-labeled H2030BrM and LL/2 cells were intracardially injected at a concentration of 2×10^5 H2030BrM cells or 5×10^4 LL/2 cells in 100 µl PBS into the left cardiac ventricle. To confirm a successful injection, the photon flux from whole body of the mice was immediately measured using IVIS Xenogen bioimager (Caliper). To examine the effect of nicotine, the mice received nicotine (1 mg/kg) by intraperitoneal injection every 3 d. To examine the role of microglia on nicotine-related brain metastasis, the mice were administered PLX3397 (20 mg in 7 µl, Selleck Chemicals USA), a selective inhibitor of CSF1R (also known as macrophage colony-stimulating factor receptor), which reduces viability of microglial cells. To avoid whole-body effect, the PLX3397 was directly injected into the right mouse brain after 1 wk of transplantation of mouse lung cancer cell LL/2. Mice were divided into four groups: (1) tumor transplant only, (2) tumor transplant plus nicotine, (3) tumor transplant plus PLX3397, and (4) tumor transplant plus PLX3397 and nicotine. To examine the effect of natural compound (PTL) on modulation of microglial cell polarization, the mice were administered PTL (1 mg/kg) plus nicotine by intraperitoneal injection. Mice were divided into three groups: (1) tumor transplant only, (2) tumor transplant plus nicotine, and (3) tumor transplant plus PTL and nicotine. Tumor growth was monitored by bioluminescence until day 60. For bioluminescent imaging, the mice were injected with D-luciferin intraperitoneally (100 mg/kg), followed by capturing images every week using IVIS Xenogen bioimager. The brain metastasis was monitored, and the luminescence was quantified once per week. Finally, whole brain was removed and incubated in PBS with 0.6 mg/ml luciferin for 5 min, and photon flux was measured by an in vivo image system (IVIS).

Intracranial implantation

Mice were anesthetized with a ketamine/xylazine (90–120/7–10 mg/kg) mixture and fixed into a stereotactic head frame (Kopf stereotactic frame). A 1.5-mm bur hole was drilled 1 mm anterior to the coronal suture on the right hemisphere and 2 mm lateral from the midline. A Hamilton syringe fixed onto the head frame was used to inject LL/2 (2×10^5 cells/5 µl) into the right frontal lobe of the brain. The skin incision was then closed with 4–0 silk thread. The ketoprofen (2 mg/kg) was given to the mice to reduce pain. After 1 wk of tumor transplantation, 36 mice were randomly divided into four groups: (1) tumor transplant only (control group), (2) tumor transplant plus nicotine, (3) tumor transplant plus PLX3397, and (4) tumor transplant plus PLX3397 and nicotine. The PLX3397 and PLX3397 plus nicotine groups received PLX3397 (20 mg in 7 µl) treatment by intracranial injection every 2 wk at the same area of tumor transplantation. The control group received the same volume of PBS.

Arg1 gene promoter reporter assay and natural compound screening

To examine the nicotine-induced M2 microglial polarization and examine the effect of natural compounds on microglial polarization, SIM-A9 cells were first infected with lentivirus containing GFP gene, and GFP^+ cells were sorted by flow cytometry (FACS). The GFP^+ SIM-A9 cells were seeded in 96-well plates for 1 d and were transfected with the Arg1 promoter reporter plasmid (Addgene) using Lipofectamine 2000 (Invitrogen). After 24 h, the cells were treated with only nicotine or nicotine plus natural compound in presence of 2% FBS and cultured for another 24 h. Cells were washed twice and were treated with D-luciferin for 5 min. The expression of luciferase was detected by using an IVIS Xenogen bioimager. For Arg1 promoter luciferase normalization, the photon flux was divided by GFP signal, which was measured by a Multi-Mode Reader (Biocompare). Each experiment was conducted a minimum of three times.

qRT-PCR

For qRT-PCR, the treated cells were washed with PBS and lysed using the TRIzol reagent. The isolated total RNA was quantified by a NanoDrop 2000 (Thermo Fisher Scientific). Then, RNA was reverse transcribed to cDNA using a Reverse Transcription Supermix kit (Bio-Rad). The cDNA was then amplified with a pair of forward and reverse primers for the following genes: hCD74-F 5′-GCGACCTTATCTCCAACAATG-3′, hCD74-R 5′-GTCCTCCAGTTCCAGTGACT-3′, hCD80-F 5′-CTCTTGGTGCTGGCTGGTCTTT-3′, hCD80-R 5′-GCCAGTAGATGCGAGTTTGTGC-3′, hCD86-F 5′-CCATCAGCTTGTCTGTTTCATTCC-3′, hCD86-R 5′-GCTGTAATCCAAGGAATGTGGTC-3′, hArginase-1-F 5′-GCGGGCGGACGCTGGCG-3′, hArginase-1-R 5′-GCAGCGGGACCATGCTCCACTC-3′, hArginase-2-F 5′-AGACGCGAGTGCATTCCATC-3′, hArginase-2-R 5′-CACTAATGGTACCGATTGCCA-3′, hCD204-F 5′-GGTTTCAATTGTAAAGAGAGAGAAG-3′, hCD204-R 5′-CTGAGCAATTCTTCGTTTCCC-3′, mCD74-F 5′-AGAGCCAGAAAGGTGCAGC-3′, mCD74-R 5′-GATGCATCACATGGTCCTGG-3′, mCD80-F 5′-ACGTATTGGAAGGAGATTACAGCT-3′, mCD80-R 5′-TCTGTCAGCGTTACTATCCCGC-3′, mCD86-F 5′-TTACGGAAGCACCCACGATG-3′, mCD86-R 5′-CCTGTTACATTCTGAGCCAGT-3′, hCHRNA7-F 5′-CGTGGATGAGAAGAACCAAG-3′, hCHRNA7-R 5′-CCATTGGGGATATAGCCACT-3′, hSOX2-F 5′-GGGAAATGGGAGGGGTGCAAAAGAGG-3′, hSOX2-R 5′-TTGCGTGAGTGTGGATGGGATTGGTG-3′, hOCT4-F 5′-GCTGGAGAAGGAGAAGCTGGAGC-3′, hOCT4-R 5′-GCTAAGCTGCAGAGCCTCAAAGC-3′, hNanog-F 5′-CTTGGAAGCTGCTGGGGAAG-3′, hNanog-R 5′-GATGGGAGGAGGGGAGAGGA-3′, hCD47-F 5′-GCTAAAATATCGTGTTGTTTCATGGTTTTC-3′, hCD47-R 5′-GCTGTACTAAACACATAGTAGTGAAGT-3′, hSIRP-F 5′-GCCTTAGTCGTTCGCCCGCG-3′, hSIRP-R 5′-GCCGGCTTGGCCCTACTCCT-3′, hIGF-1-F 5′-GCTGTGCCTGCTCACCTTCACCAG-3′, hIGF-1-R 5′-GCCTCCTTAGATCACAGCTCCGGAAG-3′, hCCL20-F 5′-TCTCGCCTCCAGCATGAAAG-3′, and hCCL20-R 5′-CAGATCTCCTTGGCCACAATG-3′.

PCR reactions were performed using iTaq Universal SYBR Green Supermix (Bio-Rad) and CFX Connect (Bio-Rad). The thermal cycling conditions composed of an initial denaturation step at 95°C for 5 min, followed by 35 cycles of PCR using the following profile: 94°C, 30 s; 60°C, 30 s; and 72°C, 30 s.

Immunocytochemistry and immunofluorescence

The human brain metastasis tissues of lung cancer were obtained from Wake Forest Baptist Comprehensive Cancer Center Tumor Tissue and Pathology Shared Resource. Tissue sections were stained using anti-CD206 (1:200, R&D Systems) for M2 microglia and anti-ionized calcium-binding adapter molecule-1 (Iba1; 1:1,000, Abcam) for microglia and CD45 (1:500, Abcam) for macrophage. Brain sections were then incubated with appropriate biotin-conjugated secondary antibodies and diaminobenzidine as the substrate. As a control, isotype antibodies were used. To examine the expression of SIRPα on microglia, 10-µm-thick frozen mouse brain sections were stained using rabbit anti-Iba1 (1:1,000; Abcam) for microglia and anti-SIRPα (1:200) (Cell Signaling). Brain sections were incubated for 1 h in a PBS solution containing 0.1% Triton X-100 and 3% bovine serum albumin at room temperature, and then transferred to a solution containing anti-SIRPα antibody overnight at 4°C. The secondary antibody conjugated with fluorescent dye Alexa Fluor 594 (1:1,000, Invitrogen) was used to detect the expression of SIRPα. Sections were then incubated overnight at 4°C in a solution containing anti-Iba1 antibodies. Antibodies against rabbit IgG conjugated with fluorescent dye Alexa Fluor 488 (1:1,000, Invitrogen) were used to detect the microglial cells. Fluorescence images were acquired using a microscope (BZ-X710, Keyence) connected to a computer equipped with imaging software (BZ-X Viewer). Appropriate isotype antibodies were used as controls. To determine the area of $Iba1^+$ and $CD206^+$ cells in brain metastasis, we chose three randomly selected fields in each tumor and measured staining intensity after taking images followed by using the Image-Pro software. We also chose three nontumor areas in the corresponding slide and measured intensity as background, and this background was subtracted from the intensity in the tumor area. The average intensity of three fields was used as the score of that patient. Therefore, each patient has a single score. We then divided the score range by setting the lowest score as 0 and the highest to be +3.

Western blot

Cells were homogenized in the radioimmunoprecipitation assay buffer and then centrifuged at 17,000 *g* for 30 min at 4°C. The protein concentrations of the supernatants were determined by NanoDrop 2000. Supernatants (30 µg of total protein) were mixed with sample buffer containing 0.5 M dithiothreitol, heated to 80°C for 10 min, loaded into each well of 10% polyacrylamide gel, and resolved at 120 V for 2 h. The separated proteins bands were transferred to a polyvinylidene fluoride membrane, blocked with 5% milk, and probed with respective primary antibodies: total-STAT3 (1:1,000, Cell Signaling), phospho-STAT3 (1:1,000, Cell Signaling), GAPDH (1:10,000, Cell Signaling), SOX2 (1:500, Cell Signaling), OCT4 (1:1,000, Cell Signaling), NANOG (1:500, Cell Signaling), and SIRPα (1:1,000, Cell Signaling). The bound antibodies were detected using an enhanced chemiluminescence detection kit (GE Healthcare Lifescience). The band intensities were measured using an imaging system (Amersham Imager 600; UVP) and analyzed using ImageJ (1.43u; http://rsb.info.nih.gov/ij/). For gel loading control, membranes were incubated with monoclonal GAPDH antibody.

CCL20 ELISA

Mouse brain specimens were homogenized in radioimmunoprecipitation assay lysis buffer and centrifuged at 13,000 *g* for 30 min at 4°C. The protein concentrations of the supernatant were measured and adjusted to 1 mg/ml. The human serum of lung cancer patients was obtained from FOX CHASE Cancer Center. The serum was further diluted fourfold in assay buffer. The levels of CCL20 in the mouse brain supernatants and mouse and human serum were determined using mouse and human CCL20 ELISA kits (Sigma-Aldrich). Briefly, 96-well plates were first coated with anti-CCL20 monoclonal antibodies followed by addition of 100 µl of the supernatants and serum under investigation or the same volume of the CCL20 standards. The plate was incubated at 4°C overnight on a rocking platform. After washing the plates, the detection antibody and streptavidin solution were added to each well. After incubation, the 3,3′,5,5′-tetramethylbenzidine (TMB) and stop solution were added to each well. Finally, the plates were examined at an absorbance wavelength of 450 nm. Standard curves were obtained from values generated from known concentrations of mouse and human CCL20 provided by the kits.

IGF-1 ELISA

Microglial cells (HMC3) were treated with or without nicotine (1 µM) plus STATTIC (0.5 µM) for 24 h. Cells were washed with PBS twice and incubated in the fresh DMEM/F12 medium supplemented with 2% FBS for an additional 24 h. The human monocyte/macrophage cells were treated with or without nicotine for 24 h. CM was collected and analyzed by the human IGF-1 ELISA kit (Sigma-Aldrich). Briefly, 96-well plates were first coated with anti–IGF-1 monoclonal antibodies followed by addition of 100 µl of the microglia conditional medium or the same volume of the IGF-1 standards. The plate was incubated at 4°C overnight on a rocking platform. After washing the plates, the detection antibody and streptavidin solution were added to each well. After incubation, the TMB and stop solution were added to each well. Finally, the plates were examined at an absorbance wavelength of 450 nm. Standard curves were obtained from values generated from known concentrations of mouse and human IGF-1 provided by the kit.

Phagocytosis assay

H2030BrM and LL/2 cells were labeled with PKH26 dye (Sigma-Aldrich). The labeled cells were then washed three times and cultured overnight to reduce nonspecific leaking of dye during the assay. Tumor cells were 95% viable after the incubation. Labeled tumor cells were mixed with microglia that were pretreated with or without nicotine. Co-cultured tumor and microglia cells in the culture slides were harvested after 24 h and fixed with 4% paraformaldehyde. Microglial cells were counterstained with anti-Iba1 antibody overnight. Secondary antibody conjugated with the fluorescent dye Alexa Fluor 488 (1:1,000, Invitrogen) was used to detect the microglia. The phagocytic activities were measured by immunofluorescence microscope and FACS. For quantification of phagocytosis, the phagocytic percentage was calculated as 100 × (percent $Iba1^+$/

PKH26$^+$ cells/[percent Iba1$^+$/PKH26$^-$ cells + percent Iba1$^+$/PKH26$^+$ cells]).

Statistical analysis

Data are represented as mean ± SD. Significance was set at $P < 0.05$. The nicotine effect on M1/M2 gene expression, effect of nicotine-derived microglial CM on tumor growth, and effect of nicotine on microglia phagocytosis ability were analyzed using the unpaired Student's *t* test. One-way ANOVA was used to analyze the effect of nicotine, PTL3397, or STATTIC treatment on M1/M2 gene polarization and tumor progression, the effect of different concentrations of IGF-1 or CCL20 on cancer progression, the effect of different natural compounds on M2 gene polarization, and the effect of nicotine or PTL treatment on M1/M2 gene polarization and cancer cell progression and nicotine effect in animal studies. Significance between groups was represented as *, $P < 0.05$; **, $P < 0.01$; and ***, $P < 0.001$.

Online supplemental material

Fig. S1 shows the effect of smoking and nicotine on brain metastasis. Fig. S2 demonstrates that the nicotine promotes brain metastasis in a mouse model. Fig. S3 shows that nicotine treatment of microglia increases secretion of CCL20 and IGF-1 followed by promotion of tumor cell stemness. Fig. S4 shows the effect of natural compounds on nicotine-mediated activity of Arg1 reporter. Fig. S5 shows PTL suppressed nicotine-promoted brain metastasis in syngeneic mouse model.

Acknowledgments

We thank Dr. Joan Massagué for providing the H2030-BrM cell line.

This work was supported by National Institutes of Health grants RO1CA173499, R01CA185650, and R01CA205067 (to K. Watabe). This research used Cancer Center Shared Resources, The Tumor Tissue and Pathology, Cell Engineering, Flow Cytometry, Biostatistics and Bioinformatics that are supported by the Comprehensive Cancer Center of the Wake Forest University National Cancer Institute, National Institutes of Health grant P30CA012197. The content is solely the responsibility of the authors and does not necessarily represent the official views of the National Cancer Institute.

Author contributions: S. Wu and K. Watabe designed the study and wrote the manuscript. S. Wu, F. Xing, and K. Wu conducted experiments and acquired, analyzed, and interpreted the data. S. Sharma, A. Tyagi, and K. Wu performed animal experiments. F. Xing and Y. Liu performed intracardiac injections. T. Lycan and A. Dothard performed clinical sample analysis. S. Wu, F. Xing, S. Sharma, A. Tyagi, K. Wu, Y. Liu, D. Zhao, R.P. Deshpande, Y. Shiozawa, T. Ahmed, W. Zhang, M. Chan, J. Ruiz, and K. Watabe reviewed and edited the manuscript and interpreted the data. K. Watabe supervised the study.

Disclosures: Dr. Shiozawa reported grants from Teva Pharmaceutical Industries outside the submitted work. Dr. Chan reported other from Elekta and other from Monteris outside the submitted work. No other disclosures were reported.

Submitted: 20 June 2019
Revised: 9 September 2019
Accepted: 2 March 2020

References

Adams, S., L.J. van der Laan, E. Vernon-Wilson, C. Renardel de Lavalette, E.A. Döpp, C.D. Dijkstra, D.L. Simmons, and T.K. van den Berg. 1998. Signal-regulatory protein is selectively expressed by myeloid and neuronal cells. *J. Immunol.* 161:1853–1859.

Ali, A., J.R. Goffin, A. Arnold, and P.M. Ellis. 2013. Survival of patients with non-small-cell lung cancer after a diagnosis of brain metastases. *Curr. Oncol.* 20:e300–e306. https://doi.org/10.3747/co.20.1481

Bacha, S., H. Cherif, D. Rabaa, S. Habibech, S. Cheikhrouhou, H. Racil, N. Chaouch, M.L. Megdiche, and A. Chabbou. 2018. Brain metastases of non-small cell lung cancer: prognostic factors and management. *Tunis. Med.* 96:165–171.

Badie, B., and J.M. Schartner. 2000. Flow cytometric characterization of tumor-associated macrophages in experimental gliomas. *Neurosurgery.* 46: 957–961, NaN–962. https://doi.org/10.1097/00006123-200004000-00035

Barnholtz-Sloan, J.S., A.E. Sloan, F.G. Davis, F.D. Vigneau, P. Lai, and R.E. Sawaya. 2004. Incidence proportions of brain metastases in patients diagnosed (1973 to 2001) in the Metropolitan Detroit Cancer Surveillance System. *J. Clin. Oncol.* 22:2865–2872. https://doi.org/10.1200/JCO.2004.12.149

Braverman, M.T.. 1999. Research on resilience and its implications for tobacco prevention. *Nicotine Tob. Res.* 1(Suppl 1):S67–S72. https://doi.org/10.1080/14622299050011621

Butowski, N., H. Colman, J.F. De Groot, A.M. Omuro, L. Nayak, P.Y. Wen, T.F. Cloughesy, A. Marimuthu, S. Haidar, A. Perry, et al. 2016. Orally administered colony stimulating factor 1 receptor inhibitor PLX3397 in recurrent glioblastoma: an Ivy Foundation Early Phase Clinical Trials Consortium phase II study. *Neuro-oncol.* 18:557–564. https://doi.org/10.1093/neuonc/nov245

Cannarile, M.A., M. Weisser, W. Jacob, A.M. Jegg, C.H. Ries, and D. Rüttinger. 2017. Colony-stimulating factor 1 receptor (CSF1R) inhibitors in cancer therapy. *J. Immunother. Cancer.* 5:53. https://doi.org/10.1186/s40425-017-0257-y

Carlisi, D., A. D'Anneo, L. Angileri, M. Lauricella, S. Emanuele, A. Santulli, R. Vento, and G. Tesoriere. 2011. Parthenolide sensitizes hepatocellular carcinoma cells to TRAIL by inducing the expression of death receptors through inhibition of STAT3 activation. *J. Cell. Physiol.* 226:1632–1641. https://doi.org/10.1002/jcp.22494

Chen, Q., A. Boire, X. Jin, M. Valiente, E.E. Er, A. Lopez-Soto, L. Jacob, R. Patwa, H. Shah, K. Xu, et al. 2016. Carcinoma-astrocyte gap junctions promote brain metastasis by cGAMP transfer. *Nature.* 533:493–498. https://doi.org/10.1038/nature18268

Chen, W., Y. Qin, D. Wang, L. Zhou, Y. Liu, S. Chen, L. Yin, Y. Xiao, X.H. Yao, X. Yang, et al. 2018. CCL20 triggered by chemotherapy hinders the therapeutic efficacy of breast cancer. *PLoS Biol.* 16. e2005869. https://doi.org/10.1371/journal.pbio.2005869

Cuccarese, M.F., J.M. Dubach, C. Pfirschke, C. Engblom, C. Garris, M.A. Miller, M.J. Pittet, and R. Weissleder. 2017. Heterogeneity of macrophage infiltration and therapeutic response in lung carcinoma revealed by 3D organ imaging. *Nat. Commun.* 8:14293. https://doi.org/10.1038/ncomms14293

da Fonseca, A.C., and B. Badie. 2013. Microglia and macrophages in malignant gliomas: recent discoveries and implications for promising therapies. *Clin. Dev. Immunol.* 2013. 264124. https://doi.org/10.1155/2013/264124

Ellis, T.L., M.T. Neal, and M.D. Chan. 2012. The role of surgery, radiosurgery and whole brain radiation therapy in the management of patients with metastatic brain tumors. *Int. J. Surg. Oncol.* 2012. 952345. https://doi.org/10.1155/2012/952345

Elmore, M.R., A.R. Najafi, M.A. Koike, N.N. Dagher, E.E. Spangenberg, R.A. Rice, M. Kitazawa, B. Matusow, H. Nguyen, B.L. West, et al. 2014. Colony-stimulating factor 1 receptor signaling is necessary for microglia viability, unmasking a microglia progenitor cell in the adult brain. *Neuron.* 82:380–397. https://doi.org/10.1016/j.neuron.2014.02.040

Feng, X., F. Szulzewsky, A. Yerevanian, Z. Chen, D. Heinzmann, R.D. Rasmussen, V. Alvarez-Garcia, Y. Kim, B. Wang, I. Tamagno, et al. 2015. Loss of CX3CR1 increases accumulation of inflammatory monocytes and promotes gliomagenesis. *Oncotarget.* 6:15077–15094. https://doi.org/10.18632/oncotarget.3730

Fidler, I.J.. 2015. The Biology of Brain Metastasis: Challenges for Therapy. *Cancer J.* 21:284–293. https://doi.org/10.1097/PPO.0000000000000126

Gaspar, L., C. Scott, M. Rotman, S. Asbell, T. Phillips, T. Wasserman, W.G. McKenna, and R. Byhardt. 1997. Recursive partitioning analysis (RPA) of prognostic factors in three Radiation Therapy Oncology Group (RTOG) brain metastases trials. *Int. J. Radiat. Oncol. Biol. Phys.* 37: 745–751. https://doi.org/10.1016/S0360-3016(96)00619-0

Gomez Perdiguero, E., K. Klapproth, C. Schulz, K. Busch, E. Azzoni, L. Crozet, H. Garner, C. Trouillet, M.F. de Bruijn, F. Geissmann, et al. 2015. Tissue-resident macrophages originate from yolk-sac-derived erythro-myeloid progenitors. *Nature*. 518:547–551. https://doi.org/10.1038/nature13989

Hartmann-Boyce, J., S.C. Chepkin, W. Ye, C. Bullen, and T. Lancaster. 2018. Nicotine replacement therapy versus control for smoking cessation. *Cochrane Database Syst. Rev.* 5. CD000146. https://doi.org/10.1002/14651858.CD000146.pub5

Hawkins, B.T., T.J. Abbruscato, R.D. Egleton, R.C. Brown, J.D. Huber, C.R. Campos, and T.P. Davis. 2004. Nicotine increases in vivo blood-brain barrier permeability and alters cerebral microvascular tight junction protein distribution. *Brain Res.* 1027:48–58. https://doi.org/10.1016/j.brainres.2004.08.043

He, B.P., J.J. Wang, X. Zhang, Y. Wu, M. Wang, B.H. Bay, and A.Y. Chang. 2006. Differential reactions of microglia to brain metastasis of lung cancer. *Mol. Med.* 12:161–170. https://doi.org/10.2119/2006-00033.He

Heishman, S.J.. 1999. Behavioral and cognitive effects of smoking: relationship to nicotine addiction. *Nicotine Tob. Res.* 1:S143–S147, NaN–S166. https://doi.org/10.1080/14622299050011971

Henningfield, J.E., C. Cohen, and J.D. Slade. 1991. Is nicotine more addictive than cocaine? *Br. J. Addict.* 86:565–569. https://doi.org/10.1111/j.1360-0443.1991.tb01809.x

Huang, Z., B. Sun, S. Wu, X. Meng, Y. Cong, G. Shen, and S. Song. 2018. A nomogram for predicting survival in patients with breast cancer brain metastasis. *Oncol. Lett.* 15:7090–7096. https://doi.org/10.3892/ol.2018.8259

Hutter, G., J. Theruvath, C.M. Graef, M. Zhang, M.K. Schoen, E.M. Manz, M.L. Bennett, A. Olson, T.D. Azad, R. Sinha, et al. 2019. Microglia are effector cells of CD47-SIRPα antiphagocytic axis disruption against glioblastoma. *Proc. Natl. Acad. Sci. USA*. 116:997–1006. https://doi.org/10.1073/pnas.1721434116

Janker, F., W. Weder, J.H. Jang, and W. Jungraithmayr. 2018. Preclinical, non-genetic models of lung adenocarcinoma: a comparative survey. *Oncotarget*. 9:30527–30538. https://doi.org/10.18632/oncotarget.25668

Kakusa, B., S. Han, S. Aggarwal, B. Liu, G. Li, S. Soltys, and M. Hayden Gephart. 2018. Clinical factors associated with mortality within three months after radiosurgery of asymptomatic brain metastases from non-small cell lung cancer. *J. Neurooncol.* 140:705–715. https://doi.org/10.1007/s11060-018-03002-0

Kamei, D., M. Murakami, Y. Sasaki, Y. Nakatani, M. Majima, Y. Ishikawa, T. Ishii, S. Uematsu, S. Akira, S. Hara, et al. 2009. Microsomal prostaglandin E synthase-1 in both cancer cells and hosts contributes to tumour growth, invasion and metastasis. *Biochem. J.* 425:361–371. https://doi.org/10.1042/BJ20090045

Kharitonenkov, A., Z. Chen, I. Sures, H. Wang, J. Schilling, and A. Ullrich. 1997. A family of proteins that inhibit signalling through tyrosine kinase receptors. *Nature*. 386:181–186. https://doi.org/10.1038/386181a0

Könczöl, A., J. Müller, E. Földes, Z. Béni, K. Végh, A. Kéry, and G.T. Balogh. 2013. Applicability of a blood-brain barrier specific artificial membrane permeability assay at the early stage of natural product-based CNS drug discovery. *J. Nat. Prod.* 76:655–663. https://doi.org/10.1021/np300882f

Lee, P.N., B.A. Forey, and K.J. Coombs. 2012. Systematic review with meta-analysis of the epidemiological evidence in the 1900s relating smoking to lung cancer. *BMC Cancer*. 12:385. https://doi.org/10.1186/1471-2407-12-385

Leskovar, A., L.J. Moriarty, J.J. Turek, I.A. Schoenlein, and R.B. Borgens. 2000. The macrophage in acute neural injury: changes in cell numbers over time and levels of cytokine production in mammalian central and peripheral nervous systems. *J. Exp. Biol.* 203(Pt 12):1783–1795.

Li, T., J. Zhang, J. Zhang, N. Zhang, Y. Zeng, S. Tang, Z. Tao, X. Qu, J. Jia, W. Zhu, et al. 2017. Nicotine-enhanced stemness and epithelial-mesenchymal transition of human umbilical cord mesenchymal stem cells promote tumor formation and growth in nude mice. *Oncotarget*. 9: 591–606. https://doi.org/10.18632/oncotarget.22712

Lin, M., H. Bi, Y. Yan, W. Huang, G. Zhang, G. Zhang, S. Tang, Y. Liu, L. Zhang, J. Ma, et al. 2017. Parthenolide suppresses non-small cell lung cancer GLC-82 cells growth via B-Raf/MAPK/Erk pathway. *Oncotarget*. 8:23436–23447. https://doi.org/10.18632/oncotarget.15584

Liu, Q., J. Zhao, R. Tan, H. Zhou, Z. Lin, M. Zheng, E. Romas, J. Xu, and N.A. Sims. 2015a. Parthenolide inhibits pro-inflammatory cytokine production and exhibits protective effects on progression of collagen-induced arthritis in a rat model. *Scand. J. Rheumatol.* 44:182–191. https://doi.org/10.3109/03009742.2014.938113

Liu, X., Y. Pu, K. Cron, L. Deng, J. Kline, W.A. Frazier, H. Xu, H. Peng, Y.X. Fu, and M.M. Xu. 2015b. CD47 blockade triggers T cell-mediated destruction of immunogenic tumors. *Nat. Med.* 21:1209–1215. https://doi.org/10.1038/nm.3931

Liu, B., Y. Jia, J. Ma, S. Wu, H. Jiang, Y. Cao, X. Sun, X. Yin, S. Yan, M. Shang, et al. 2016. Tumor-associated macrophage-derived CCL20 enhances the growth and metastasis of pancreatic cancer. *Acta Biochim. Biophys. Sin. (Shanghai)*. 48:1067–1074. https://doi.org/10.1093/abbs/gmw101

Liu, M., C. Xiao, M. Sun, M. Tan, L. Hu, and Q. Yu. 2018. Parthenolide Inhibits STAT3 Signaling by Covalently Targeting Janus Kinases. *Molecules*. 23. E1478. https://doi.org/10.3390/molecules23061478

Lu, E., J. Su, Y. Zhou, C. Zhang, and Y. Wang. 2017. CCL20/CCR6 promotes cell proliferation and metastasis in laryngeal cancer by activating p38 pathway. *Biomed. Pharmacother.* 85:486–492. https://doi.org/10.1016/j.biopha.2016.11.055

Malladi, S., D.G. Macalinao, X. Jin, L. He, H. Basnet, Y. Zou, E. de Stanchina, and J. Massagué. 2016. Metastatic Latency and Immune Evasion through Autocrine Inhibition of WNT. *Cell*. 165:45–60. https://doi.org/10.1016/j.cell.2016.02.025

Marsigliante, S., C. Vetrugno, and A. Muscella. 2016. Paracrine CCL20 loop induces epithelial-mesenchymal transition in breast epithelial cells. *Mol. Carcinog.* 55:1175–1186. https://doi.org/10.1002/mc.22360

Mazzaferro, S., I. Bermudez, and S.M. Sine. 2017. α4β2 Nicotinic Acetylcholine Receptors: Relationships Between Subunit Stoichiometry and Function at the Single Channel Level. *J. Biol. Chem.* 292:2729–2740. https://doi.org/10.1074/jbc.M116.764183

Morioka, N., S. Harano, M. Tokuhara, Y. Idenoshita, F.F. Zhang, K. Hisaoka-Nakashima, and Y. Nakata. 2015. Stimulation of α7 nicotinic acetylcholine receptor regulates glutamate transporter GLAST via basic fibroblast growth factor production in cultured cortical microglia. *Brain Res.* 1625:111–120. https://doi.org/10.1016/j.brainres.2015.08.029

Mujoomdar, A., J.H. Austin, R. Malhotra, C.A. Powell, G.D. Pearson, M.C. Shiau, and H. Raftopoulos. 2007. Clinical predictors of metastatic disease to the brain from non-small cell lung carcinoma: primary tumor size, cell type, and lymph node metastases. *Radiology*. 242:882–888. https://doi.org/10.1148/radiol.2423051707

Munn, D.H., and N.K. Cheung. 1990. Phagocytosis of tumor cells by human monocytes cultured in recombinant macrophage colony-stimulating factor. *J. Exp. Med.* 172:231–237. https://doi.org/10.1084/jem.172.1.231

Nandi, B., C. Pai, Q. Huang, R.H. Prabhala, N.C. Munshi, and J.S. Gold. 2014. CCR6, the sole receptor for the chemokine CCL20, promotes spontaneous intestinal tumorigenesis. *PLoS One*. 9. e97566. https://doi.org/10.1371/journal.pone.0097566

Nguyen, D.X., A.C. Chiang, X.H. Zhang, J.Y. Kim, M.G. Kris, M. Ladanyi, W.L. Gerald, and J. Massagué. 2009. WNT/TCF signaling through LEF1 and HOXB9 mediates lung adenocarcinoma metastasis. *Cell*. 138:51–62. https://doi.org/10.1016/j.cell.2009.04.030

Pan, Y.F., Y.X. Tan, M. Wang, J. Zhang, B. Zhang, C. Yang, Z.W. Ding, L.W. Dong, and H.Y. Wang. 2013. Signal regulatory protein α is associated with tumor-polarized macrophages phenotype switch and plays a pivotal role in tumor progression. *Hepatology*. 58:680–691. https://doi.org/10.1002/hep.26391

Park, Y.S., D.J. Kim, H. Koo, S.H. Jang, Y.M. You, J.H. Cho, S.J. Yang, E.S. Yu, Y. Jung, D.C. Lee, et al. 2016. AKT-induced PKM2 phosphorylation signals for IGF-1-stimulated cancer cell growth. *Oncotarget*. 7: 48155–48167. https://doi.org/10.18632/oncotarget.10179

Prinz, M., and J. Priller. 2014. Microglia and brain macrophages in the molecular age: from origin to neuropsychiatric disease. *Nat. Rev. Neurosci.* 15:300–312. https://doi.org/10.1038/nrn3722

Qin, C., W.H. Fan, Q. Liu, K. Shang, M. Murugan, L.J. Wu, W. Wang, and D.S. Tian. 2017. Fingolimod Protects Against Ischemic White Matter Damage by Modulating Microglia Toward M2 Polarization via STAT3 Pathway. *Stroke*. 48:3336–3346. https://doi.org/10.1161/STROKEAHA.117.018505

Redmer, T.. 2018. Deciphering mechanisms of brain metastasis in melanoma - the gist of the matter. *Mol. Cancer*. 17:106. https://doi.org/10.1186/s12943-018-0854-5

Roesch, S., C. Rapp, S. Dettling, and C. Herold-Mende. 2018. When Immune Cells Turn Bad-Tumor-Associated Microglia/Macrophages in Glioma. *Int. J. Mol. Sci.* 19. E436. https://doi.org/10.3390/ijms19020436

Rummel, C., R. Gerstberger, J. Roth, and T. Hübschle. 2011. Parthenolide attenuates LPS-induced fever, circulating cytokines and markers of brain inflammation in rats. *Cytokine*. 56:739–748. https://doi.org/10.1016/j.cyto.2011.09.022

Sadigh-Eteghad, S., A. Majdi, J. Mahmoudi, S.E.J. Golzari, and M. Talebi. 2016. Astrocytic and microglial nicotinic acetylcholine receptors: an overlooked issue in Alzheimer's disease. *J. Neural Transm. (Vienna)*. 123:1359–1367. https://doi.org/10.1007/s00702-016-1580-z

Schaal, C., and S.P. Chellappan. 2014. Nicotine-mediated cell proliferation and tumor progression in smoking-related cancers. *Mol. Cancer Res*. 12:14–23. https://doi.org/10.1158/1541-7786.MCR-13-0541

Schaal, C.M., N. Bora-Singhal, D.M. Kumar, and S.P. Chellappan. 2018. Regulation of Sox2 and stemness by nicotine and electronic-cigarettes in non-small cell lung cancer. *Mol. Cancer*. 17:149. https://doi.org/10.1186/s12943-018-0901-2

Scholar, E.M., L.A. Violi, J. Newland, E. Bresnick, and D.F. Birt. 1989. The effect of dietary fat on metastasis of the Lewis lung carcinoma and the BALB/c mammary carcinoma. *Nutr. Cancer*. 12:109–119. https://doi.org/10.1080/01635588909514009

Schouten, L.J., J. Rutten, H.A. Huveneers, and A. Twijnstra. 2002. Incidence of brain metastases in a cohort of patients with carcinoma of the breast, colon, kidney, and lung and melanoma. *Cancer*. 94:2698–2705. https://doi.org/10.1002/cncr.10541

Schulz, C., E. Gomez Perdiguero, L. Chorro, H. Szabo-Rogers, N. Cagnard, K. Kierdorf, M. Prinz, B. Wu, S.E. Jacobsen, J.W. Pollard, et al. 2012. A lineage of myeloid cells independent of Myb and hematopoietic stem cells. *Science*. 336:86–90. https://doi.org/10.1126/science.1219179

Scott, A., S.T. Lugg, K. Aldridge, K.E. Lewis, A. Bowden, R.Y. Mahida, F.S. Grudzinska, D. Dosanjh, D. Parekh, R. Foronjy, et al. 2018. Pro-inflammatory effects of e-cigarette vapour condensate on human alveolar macrophages. *Thorax*. 73(12):1161–1169. https://doi.org/10.1136/thoraxjnl-2018-211663

Shenker, R.F., E.R. McTyre, J. Ruiz, K.E. Weaver, C. Cramer, N.K. Alphonse-Sullivan, M. Farris, W.J. Petty, M.R. Bonomi, K. Watabe, et al. 2017. The Effects of smoking status and smoking history on patients with brain metastases from lung cancer. *Cancer Med*. 6:944–952. https://doi.org/10.1002/cam4.1058

Skoumal, R., M. Tóth, R. Serpi, J. Rysä, H. Leskinen, J. Ulvila, T. Saiho, J. Aro, H. Ruskoaho, I. Szokodi, et al. 2011. Parthenolide inhibits STAT3 signaling and attenuates angiotensin II-induced left ventricular hypertrophy via modulation of fibroblast activity. *J. Mol. Cell. Cardiol*. 50:634–641. https://doi.org/10.1016/j.yjmcc.2011.01.001

Sobota, R., M. Szwed, A. Kasza, M. Bugno, and T. Kordula. 2000. Parthenolide inhibits activation of signal transducers and activators of transcription (STATs) induced by cytokines of the IL-6 family. *Biochem. Biophys. Res. Commun*. 267:329–333. https://doi.org/10.1006/bbrc.1999.1948

Song, J.M., X. Qian, P. Upadhyayya, K.H. Hong, and F. Kassie. 2014. Dimethylaminoparthenolide, a water soluble parthenolide, suppresses lung tumorigenesis through down-regulating the STAT3 signaling pathway. *Curr. Cancer Drug Targets*. 14:59–69. https://doi.org/10.2174/1568009613136660108

Sperduto, P.W., B. Berkey, L.E. Gaspar, M. Mehta, and W. Curran. 2008. A new prognostic index and comparison to three other indices for patients with brain metastases: an analysis of 1,960 patients in the RTOG database. *Int. J. Radiat. Oncol. Biol. Phys*. 70:510–514. https://doi.org/10.1016/j.ijrobp.2007.06.074

Stead, L.F., R. Perera, C. Bullen, D. Mant, J. Hartmann-Boyce, K. Cahill, and T. Lancaster. 2012. Nicotine replacement therapy for smoking cessation. *Cochrane Database Syst. Rev*. 11. CD000146. https://doi.org/10.1002/14651858.CD000146.pub4

Sun, H.J., Y.F. Jia, and X.L. Ma. 2017. Alpha5 Nicotinic Acetylcholine Receptor Contributes to Nicotine-Induced Lung Cancer Development and Progression. *Front. Pharmacol*. 8:573. https://doi.org/10.3389/fphar.2017.00573

Talib, W.H., and L.T. Al Kury. 2018. Parthenolide inhibits tumor-promoting effects of nicotine in lung cancer by inducing P53 - dependent apoptosis and inhibiting VEGF expression. *Biomed. Pharmacother*. 107:1488–1495. https://doi.org/10.1016/j.biopha.2018.08.139

Verger, E., M. Gil, R. Yaya, N. Viñolas, S. Villà, T. Pujol, L. Quintó, and F. Graus. 2005. Temozolomide and concomitant whole brain radiotherapy in patients with brain metastases: a phase II randomized trial. *Int. J. Radiat. Oncol. Biol. Phys*. 61:185–191. https://doi.org/10.1016/j.ijrobp.2004.04.061

Wang, G.Z., X. Cheng, X.C. Li, Y.Q. Liu, X.Q. Wang, X. Shi, Z.Y. Wang, Y.Q. Guo, Z.S. Wen, Y.C. Huang, et al. 2015. Tobacco smoke induces production of chemokine CCL20 to promote lung cancer. *Cancer Lett*. 363:60–70. https://doi.org/10.1016/j.canlet.2015.04.005

Wang, B., L. Shi, X. Sun, L. Wang, X. Wang, and C. Chen. 2016. Production of CCL20 from lung cancer cells induces the cell migration and proliferation through PI3K pathway. *J. Cell. Mol. Med*. 20:920–929. https://doi.org/10.1111/jcmm.12781

Wang, C., W. Gu, Y. Zhang, Y. Ji, Y. Wen, and X. Xu. 2017. Nicotine promotes cervical carcinoma cell line HeLa migration and invasion by activating PI3k/Akt/NF-κB pathway in vitro. *Exp. Toxicol. Pathol*. 69:402–407. https://doi.org/10.1016/j.etp.2017.03.006

Wei, J., K. Gabrusiewicz, and A. Heimberger. 2013. The controversial role of microglia in malignant gliomas. *Clin. Dev. Immunol*. 2013. 285246. https://doi.org/10.1155/2013/285246

Wu, S.Y., and K. Watabe. 2017. The roles of microglia/macrophages in tumor progression of brain cancer and metastatic disease. *Front. Biosci*. 22:1805–1829. https://doi.org/10.2741/4573

Xing, F., Y. Liu, S.Y. Wu, K. Wu, S. Sharma, Y.Y. Mo, J. Feng, S. Sanders, G. Jin, R. Singh, et al. 2018. Loss of XIST in Breast Cancer Activates MSN-c-Met and Reprograms Microglia via Exosomal miRNA to Promote Brain Metastasis. *Cancer Res*. 78:4316–4330. https://doi.org/10.1158/0008-5472.CAN-18-1102

Yi, W.J., and T.S. Kim. 2017. Melatonin protects mice against stress-induced inflammation through enhancement of M2 macrophage polarization. *Int. Immunopharmacol*. 48:146–158. https://doi.org/10.1016/j.intimp.2017.05.006

Yoneyama, R., K. Aoshiba, K. Furukawa, M. Saito, H. Kataba, H. Nakamura, and N. Ikeda. 2016. Nicotine enhances hepatocyte growth factor-mediated lung cancer cell migration by activating the α7 nicotine acetylcholine receptor and phosphoinositide kinase-3-dependent pathway. *Oncol. Lett*. 11:673–677. https://doi.org/10.3892/ol.2015.3930

Zhang, S., and T.M. Petro. 1996. The effect of nicotine on murine CD4 T cell responses. *Int. J. Immunopharmacol*. 18:467–478. https://doi.org/10.1016/S0192-0561(96)00054-9

Zhu, C., X. Qi, Y. Chen, B. Sun, Y. Dai, and Y. Gu. 2011. PI3K/Akt and MAPK/ERK1/2 signaling pathways are involved in IGF-1-induced VEGF-C up-regulation in breast cancer. *J. Cancer Res. Clin. Oncol*. 137:1587–1594. https://doi.org/10.1007/s00432-011-1049-2

Zhu, Y., B.L. Knolhoff, M.A. Meyer, T.M. Nywening, B.L. West, J. Luo, A. Wang-Gillam, S.P. Goedegebuure, D.C. Linehan, and D.G. DeNardo. 2014. CSF1/CSF1R blockade reprograms tumor-infiltrating macrophages and improves response to T-cell checkpoint immunotherapy in pancreatic cancer models. *Cancer Res*. 74:5057–5069. https://doi.org/10.1158/0008-5472.CAN-13-3723

Supplemental material

	Adenocarcinoma	Non-adenocarcinoma
Age	62.78	65.21
Male gender (%)	94 (33%)	60 (21%)
Smoking status		
-Never/Former	149	73
-Current	43	16
Pack years		
<20	81	23
20-60	88	38
>60	23	28

Figure S1. **Effect of smoking and nicotine on brain metastasis.** Patient profile and their smoking history.

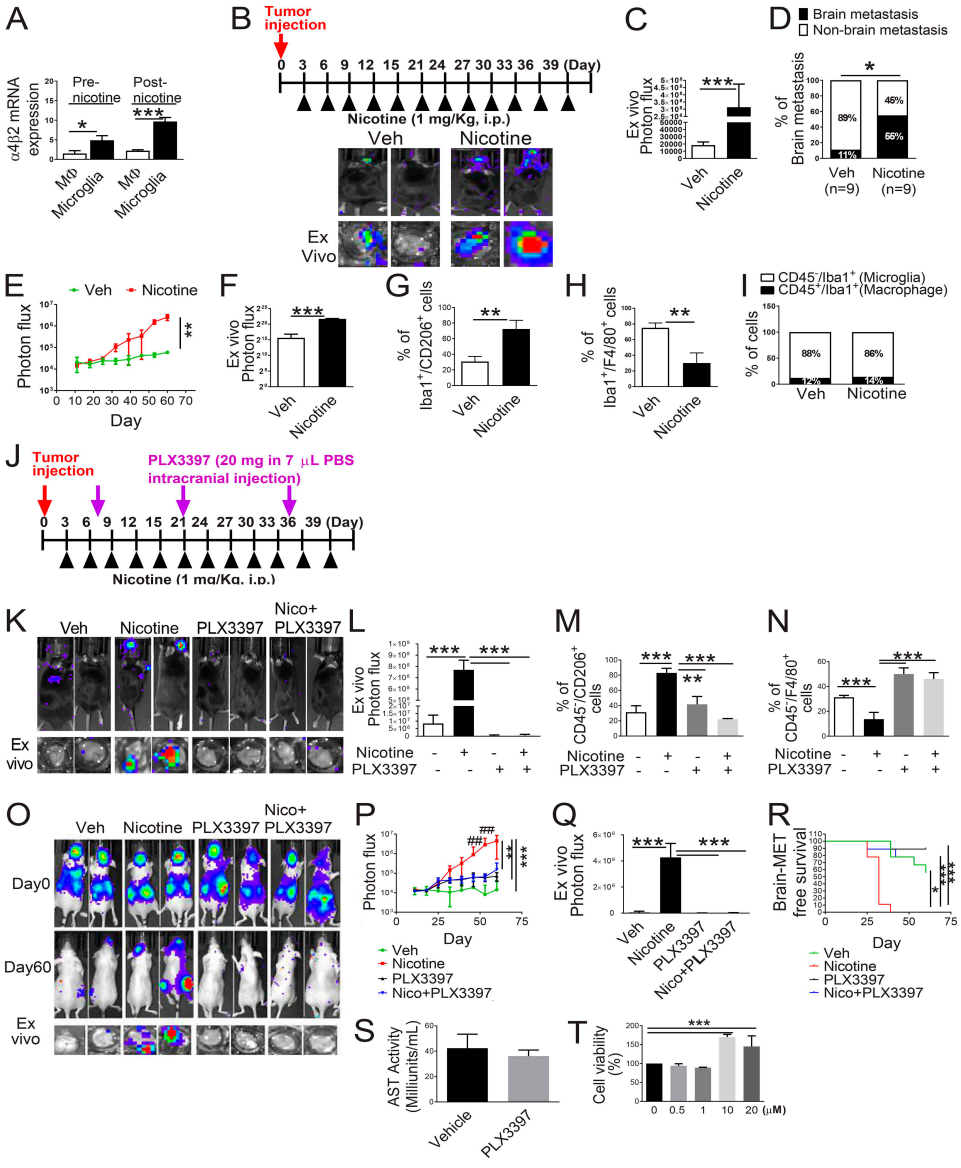

Figure S2. **Nicotine promotes brain metastasis in mouse model. (A)** Expression of the *α4β2* nicotine receptor on human microglia (HMC3) and human monocyte/macrophage (THP-1) were evaluated before and after nicotine treatment by qRT-PCR (n = 4/group). **(B)** Mouse lung cancer LL/2 cells were intracardially injected into wild-type C57BL/6 mice (n = 9/group). After 3 d of intracardiac transplantation of LL/2 cells, mice received nicotine (1 mg/kg) treatment by intraperitoneal injection every 3 d. Upper panels are BLI images of brain metastatic lesions of representative mice from each experimental group at day 40. The lower panels represent the total photon flux of ex vivo brain metastatic lesions as measured by BLI at the endpoint (day 40). **(C)** Quantitative data of in vivo brain metastasis of lung cancer (n = 9/group). **(D)** Percentage of brain metastasis of lung cancer in C57BL/6 mice with or without nicotine treatment (n = 9/group). **(E and F)** Quantitative data of in vivo brain metastasis of lung cancer (left panel) and ex vivo signals in the brain at the end point (right panel) of the experiment conducted in Fig. 2 B (n = 9/group). **(G and H)** Metastatic brain tumor tissues in Fig. 2 B were dissociated, and the effect of nicotine was examined on Iba1$^+$/CD206$^+$ (G) or Iba1$^+$/F4/80$^+$ cells (H) by FACS (n = 9/group). **(I)** Metastatic brain tumor tissues in Fig. 2 B were dissociated, and the Iba1$^+$/CD45$^-$ (microglia) and Iba1$^+$/CD45$^+$ (macrophage) were measured and plotted in relation to the nicotine treatment (n = 9/group). **(J)** Scheme of the experimental design. After 3 d of intracranial transplantation of LL/2 cells, the mice received nicotine (1 mg/kg) by intraperitoneal injection every 3 d. After 1 wk of tumor transplantation, PLX3397 (20 mg/kg in 7 µl PBS) was directly injected into the right brain of the mice every 2 wk. **(K)** Upper panels are BLI images of brain metastatic lesions of representative mice from each experimental group at day 40. The lower panels represent the total photon flux of ex vivo brain metastatic lesions as measured by BLI at the endpoint (day 40; n = 9/group). **(L)** Quantitative data of ex vivo brain metastasis of lung cancer at the end point. **(M and N)** Metastatic brain tumors in K were isolated from the brain and examined by FACS for M2 (M) and M1 (N) microglial polarization (n = 9/group). **(O)** H2030BrM (2×10^5 cells) were intracardially injected into nude mice (n = 9/group) followed by administering them with nicotine plus PLX3397 (1 mg/kg) by intraperitoneal injection every 3 d. Upper and middle panels are BLI images of brain metastatic lesions of representative mice from each experimental group at day 0 and day 60, respectively. Lower panels represent the total photon flux of ex vivo brain metastatic lesions as measured by BLI at the endpoint (day 60; n = 9/group). **(P and Q)** Quantitative data of in vivo brain metastasis of lung cancer and (Q) ex vivo signals in the brain at the end point (day 60; n = 9/group). **(R)** Kaplan–Meier analysis of brain metastasis–free survival was performed. **(S)** Serum of mice in Fig. 2 E was collected, and an aspartate aminotransferase test (AST) was measured using the AST activity assay kit (Sigma-Aldrich) (n = 9/group). **(T)** H2030BrM cells were incubated with the indicated concentration of nicotine for 24 h. They were then examined for cell viability (n = 9/group). The data are presented as the mean ± SD. *, $P < 0.05$; **, $P < 0.01$; and ***, $P < 0.001$ versus respective nicotine group. ##, $P < 0.01$ versus respective PLX3397 and Nico+PLX3397 groups.

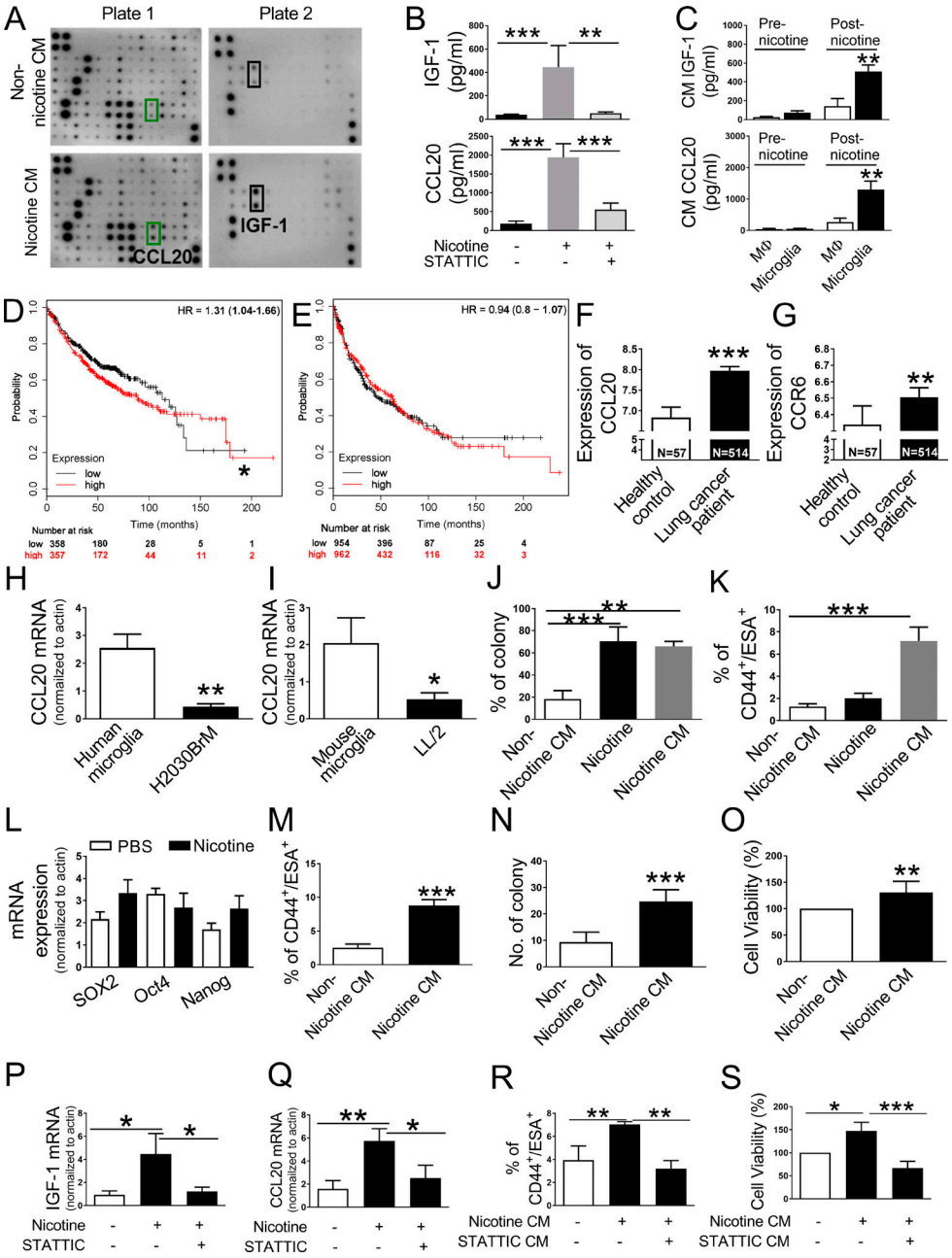

Figure S3. **Nicotine treatment of microglia increases secretion of CCL20 and IGF-1 followed by promotion of tumor cell stemness. (A)** Human microglial (HMC3) cells were treated with PBS or nicotine (1 μM) for 24 h. CM was collected and analyzed by using the cytokine/growth factor array (Raybio). **(B)** Human microglial (HMC3) cells were treated with or without nicotine (1 μM) plus STATTIC (0.5 μM) for 24 h. Cells were washed with PBS twice and incubated in the fresh DMEM/F12 medium supplemented with 2% FBS for additional 24 h. CM was collected and analyzed by IGF-1 and CCL20 ELISA (n = 4/group). **(C)** Human microglial (HMC3) cells and macrophage (THP-1) were treated with or without nicotine (1 μM) for 24 h. Cells were washed with PBS twice and incubated in the fresh DMEM/F12 medium supplemented with 2% FBS for an additional 24 h. CM was collected and analyzed by IGF-1 and CCL20 ELISA (n = 4/group). **(D and E)** Kaplan–Meier analysis was performed for examining relapse-free survival of lung cancer patients in relation to *CCL20* (P = 0.02; D) and *IGF-1* (P = 0.36; E) expression using the TCGA dataset. **(F and G)** Expressions of *CCL20* (F) and *CCR6* (G) were examined in lung tumor tissues from healthy individual and lung cancer patients using the GEO dataset (GSE22220). **(H and I)** Expression of *CCL20* in human microglia and tumor cells (H) or mouse microglia and mouse tumor cells (I) were examined by qRT-PCR (n = 4/group). **(J–L)** H2030BrM cells were treated with or without nicotine or CM extracted from human microglia that were treated with nicotine for 24 h. These cells were examined for their colony-forming ability (J), $CD44^+/ESA^+$ CSC population (K), and mRNA expression of stemness-related genes (L; n = 4/group). **(M)** Effect of CM extracted from nicotine-treated mouse microglial cells on LL/2 mouse lung CSC population was examined by FACS. **(N)** Colony-forming ability of LL/2 was measured in the presence or absence of the CM derived from nicotine-treated microglia by qRT-PCR (n = 4/group). **(O)** LL/2 cells were incubated with the CM derived from nicotine-treated microglia for 24 h. They were then examined for cell viability (n = 4/group). **(P and Q)** Mouse microglia cells were treated with or without nicotine in the presence or absence of STAT3 inhibitor for 24 h. Cells were then examined for the expression of *IGF-1* (P) or *CCL20* (Q) by qRT-PCR. LL/2 cells were treated with CM derived from microglia that were treated with or without nicotine and/or STATTIC for 24 h (n = 4/group). **(R and S)** The cells were then examined for $CD44^+/ESA^+$ CSC population (R) and for cell viability (S; n = 4/group). The data are presented as the mean ± SD. *, P < 0.05; **, P < 0.01; and ***, P < 0.001.

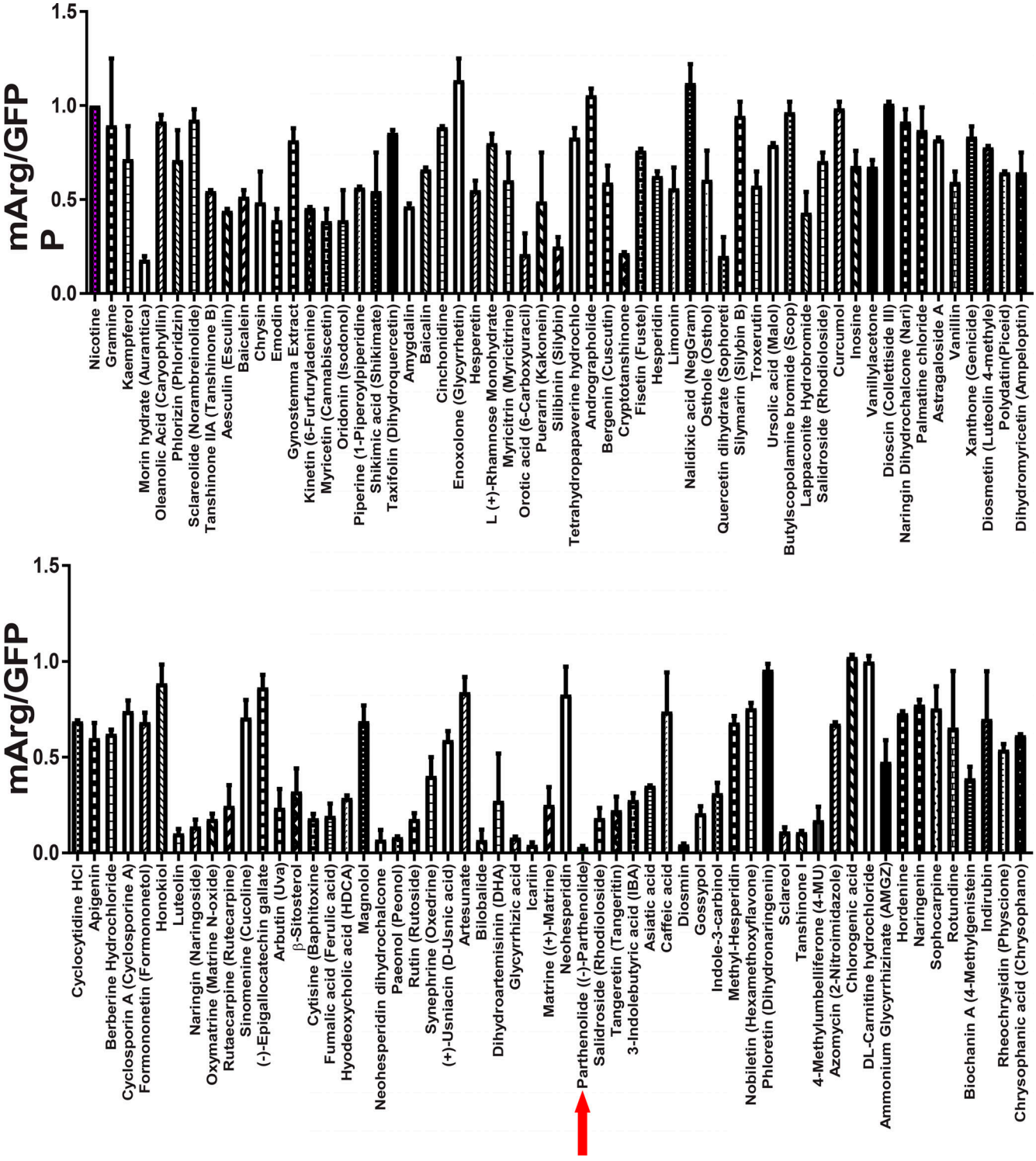

Figure S4. **Effect of natural compounds on nicotine-mediated activity of Arg1.** HMC3 cells containing Arg1 reporter plasmid were cultured in the presence or absence of nicotine (1 μM) and/or each natural compound for 24 h. These cells were then examined for direct effect of compound on nicotine-mediated activity of Arg1 reporter (n = 4/group).

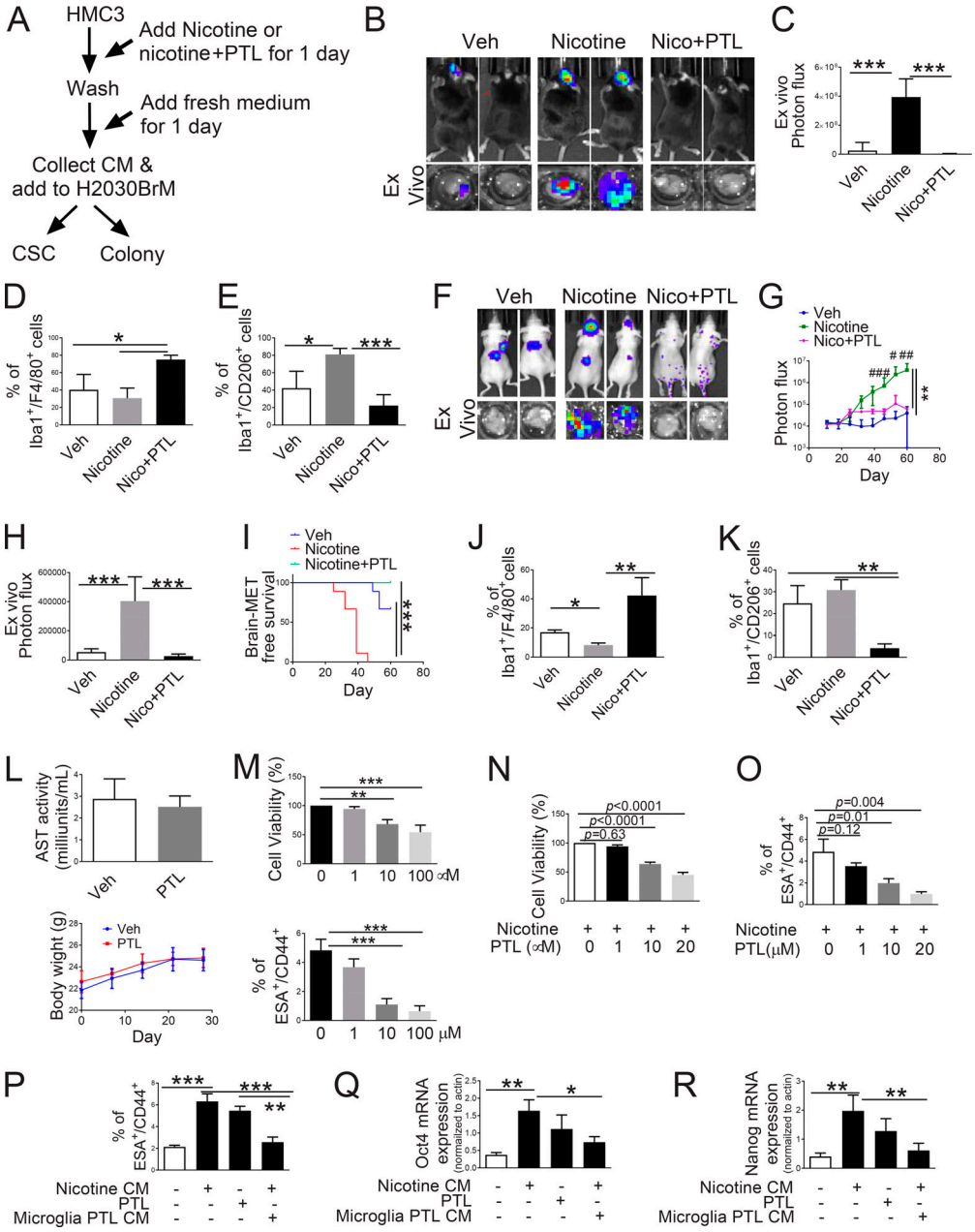

Figure S5. **PTL suppressed nicotine-promoted brain metastasis in syngeneic mouse model. (A)** Scheme of the experimental design. **(B)** Mouse lung cancer LL/2 cells were intracardially injected into wild-type C57BL/6 mice (n = 9/group) followed by administering nicotine (1 mg/kg) or PTL (1 mg/kg) by intraperitoneal injection every 3 d after tumor injection. Upper panels are BLI images of brain metastatic lesions of representative mice from each experimental group at day 40. Lower panels represent the total photon flux of ex vivo brain metastatic lesions as measured by BLI at the end point (day 40). **(C)** Quantitative data of ex vivo brain metastasis of lung cancer in the brain at the end point of the experiment conducted in B (n = 9/group). **(D and E)** Metastatic brain tumor tissues in B were dissociated and the effect of nicotine was examined for Iba1$^+$/F4/80$^+$ (D) and Iba1$^+$/CD206$^+$ (E) by FACS (n = 9/group). **(F)** H2030BrM (2×10^5 cells) were intracardially injected into nude mice followed by administering them with nicotine (1 mg/kg) plus PTL (1 mg/kg) by an intraperitoneal injection every 3 d for 60 d. Upper panel: BLI images of brain metastatic lesions of representative mice from each experimental group at day 60. Lower panel: total photon flux of ex vivo brain metastatic lesions was measured by BLI at the endpoint (day 60; n = 9/group). **(G)** Quantitative data of brain metastasis of lung cancer in vivo are shown (n = 9/group). **(H)** Ex vivo signals in the brain at the end point were examined (n = 9/group). **(I)** The Kaplan–Meier analysis of brain metastasis–free survival was performed. (n = 9/group). **(J and K)** Metastatic brain tumors were isolated from the brain and were examined by FACS for M1 (J) and M2 (K) microglial polarization using FACS (n = 5/group). **(L)** Serum of mice in Fig. 6 I was collected, and AST was measured by AST activity assay kit (Sigma-Aldrich). Body weight of the mice was also measured at the indicated time points (n = 9/group). **(M)** Direct effect of PTL on tumor cell viability by MTS assay and ESA$^+$/CD44$^+$ CSC population by FACS (n = 4/group). **(N and O)** H2030 cells were cultured in the presence or absence of nicotine (1 μM) and PTL at various concentrations for 24 h. These cells were then examined for direct effect of PTL on cell viability by MTS assay (N) and on ESA$^+$/CD44$^+$ CSC population by FACS (O; n = 4/group). **(P)** H2030BrM cells were incubated with CM derived from microglia that were treated with or without nicotine and/or PTL (1 μM) for 24 h, followed by examination of ESA$^+$/CD44$^+$ CSC population by FACS (n = 4/group). **(Q and R)** The same set of samples in P was examined for the expression of stemness-related genes, *OCT4* (Q) and *NANOG* (R), by qRT-PCR (n = 4/group). The data are presented as the mean ± SD. *, P < 0.05; **, P < 0.01; and ***, P < 0.001. #, P < 0.05; ##, P < 0.01; and ###, P < 0.001 versus respective Nico+PTL group.